

SO₃H-Functionalized Epoxy-Immobilized Fe₃O₄ Core–Shell Magnetic Nanoparticles as an Efficient, Reusable, and Eco-Friendly Catalyst for the Sustainable and Green Synthesis of Pyran and Pyrrolidinone Derivatives

Fatemeh Kalantari, Hussein Esmailipour, Hamideh Ahankar, Ali Ramazani,* Hamideh Aghahosseini, Oskar Kaszubowski, and Katarzyna Slepokura



Cite This: *ACS Omega* 2023, 8, 25780–25798



Read Online

ACCESS |



Metrics & More

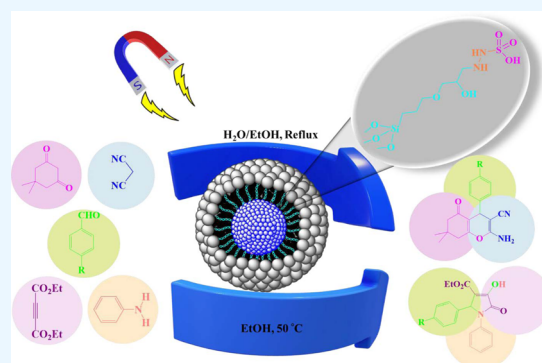


Article Recommendations



Supporting Information

ABSTRACT: A SO₃H-functionalized epoxy-immobilized Fe₃O₄ core–shell magnetic nanocatalyst was prepared through a simple three-step procedure, and it was identified by various analyses such as Fourier transform infrared (FT-IR) spectroscopy, scanning electron microscopy (SEM), differential thermal gravity (DTG), Brunauer–Emmett–Teller (BET) analysis, transmission electron microscopy (TEM), energy-dispersive X-ray spectroscopy (EDX), thermogravimetric analysis (TGA), vibration sample magnetometry (VSM), and powder X-ray diffraction (PXRD). BET analysis showed that the as-prepared nanocatalyst was synthesized with a mesoporous structure and high specific area (35.45 m² g⁻¹). The TEM image clearly showed that the particle size distribution was in the range of 47–65 nm. The designed magnetic nanocatalyst was used successfully in the synthesis of pyran derivatives via the reaction of dimedone, malononitrile, and various aromatic aldehydes and synthesis of pyrrolidinone derivatives via the reaction of various aromatic aldehydes, aniline, and diethyl acetylenedicarboxylate. The nanocatalyst was simply isolated from the reaction mixture utilizing an external magnet and reused several times according to the model reactions without significant loss in its efficiency.



1. INTRODUCTION

The most widely used magnetic nanoparticles (MNPs) are core–shell magnetite (Fe₃O₄) nanocomposites, which have been used for a variety of applications, including microwave absorption, information storage, medical diagnosis, catalysis, and color imaging.^{1,2} Recently, due to their high stability, low toxicity, and high surface area, magnetic nanoparticles, as a notable type of reusable material, have drawn considerable attention among researchers in materials science for the preparation of organic compounds.^{3,4} The high sensitivity of magnetic nanoparticles to accumulation and oxidation is due to their high surface-to-volume ratio and high chemical reactivity, which can be overcome by covering the surface of these nanoparticles with all kind of supports.⁵ In recent years, effective catalytic processes, as modified magnetic nanoparticles have been applied in several chemical advances.^{6,7} Due to the great importance of magnetic catalysts used in the synthesis of valuable materials and organic conversions, simple recovery of catalysts and reusability in several runs with a slight reduction of their magnetic nature are two prominent features in catalytic systems.^{8,9} Homogeneous Lewis and Brønsted acids are strongly favored by chemists due to their wide and varied catalytic applications in industrial and chemical processes.¹⁰ Many

organic processes have been catalyzed through some homogeneous acid catalysts such as sulfonic acid comprising materials, metal complexes, biocatalysts, metal ions, hydrogen halides, and organic metal complexes.^{11,12} However, most of these methodologies have some drawbacks such as recovery and separation problems, low thermal stability, harsh reaction conditions, and agglomeration during the reaction process. Accordingly, the major challenge of green chemistry processes is the replacement of expensive, hazardous, and polluting acidic catalysts with recyclable, environmentally friendly, and highly stable heterogeneous catalysts. Owing to the increase in the surface area of nanoparticles, they have become one of the most marvelous and significant support for acid catalysts.^{13,14}

Sulfonic acid has been proven to be one of the strongest and most popular acids that have been grafted to Fe₃O₄ nanoparticles and widely applied in various organic conversions.^{15,16}

Received: February 16, 2023

Accepted: June 14, 2023

Published: July 3, 2023



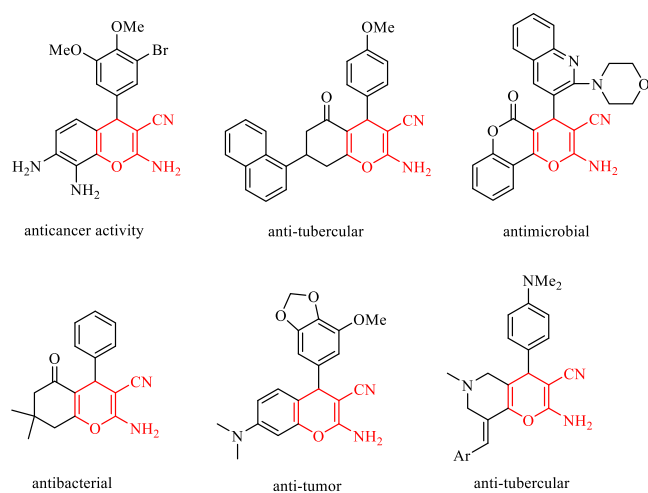


Figure 1. Selected examples of biologically active molecules based on 4H-pyran.

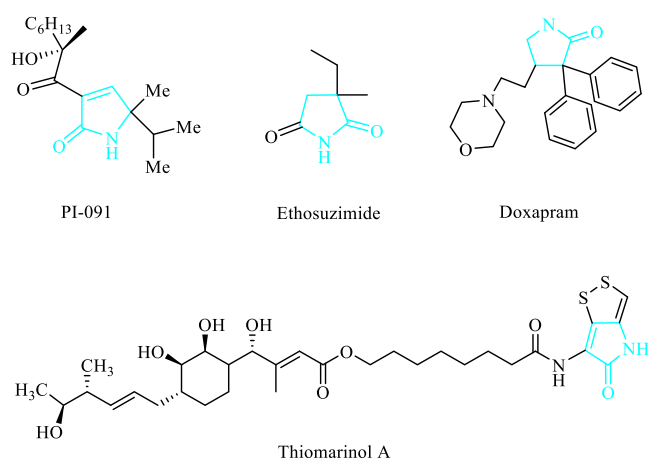


Figure 2. Selected drugs containing the 2-pyrrolidinone moiety.

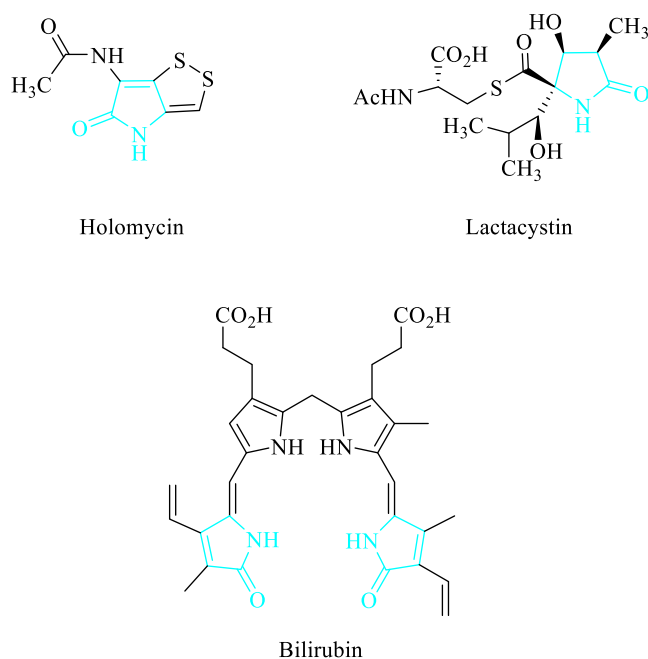


Figure 3. Selected examples of natural products containing the 2-pyrrolidinone moiety.

The sulfonic acid group chemical bond on MNPs is attained through diverse procedures such as the stabilization of perfluorosulfonic acid triethoxysilanes, oxidation of immobilized thiols, and hydrolysis of sulfonic acid chlorides.^{15–17} Several catalysts have been recently expanded, including $\text{Fe}_3\text{O}_4@ \text{Fe}_2\text{O}_3\text{-OSO}_3\text{H}$,¹⁵ $\text{SiMNP-FSO}_3\text{H}$,¹⁸ $\text{Fe}_3\text{O}_4@ \text{MCM-48-OSO}_3\text{H}$,¹⁹ $\text{Fe}_3\text{O}_4@ \text{SiO}_2@ \text{PrSO}_3\text{H}$,²⁰ and $\text{SiMNP-SO}_3\text{H}$.²¹

Although recent sulfonic acid supported catalytic systems bear important advantages compared with their homogeneous counterparts, such as reusability and recoverability nevertheless, most of them have been utilized at high temperatures and in high loading.^{22–25} In addition, since these are not lipophilic in nature, the diffusion of organic substrates on their surface is low. Hence, one of the most important issues among chemists is the design and synthesis of heterogeneous magnetic hybrid organic–inorganic NP-functionalized powerful HSO_3 groups. Of course, over recent years multicomponent reactions have received remarkable attention and have turned into a highly active field of research that provides new chemical scaffolds in one step and is also ecologically and economically attractive.^{26–28}

Tetrahydrobenzo[*b*]pyrans as one of the most significant compounds in organic chemistry are synthesized by applying MCRs with special biological and medicinal activities, including anticoagulant, anti-cancer, anti-anaphylactic, and antispasmodic, which have found an acceptable place as synthetic agents.²⁹

Figure 1 illustrates some 4H-pyran derivatives with strong pharmacological activity.³⁰ Thus, they are used as cognitive enhancers to treat neurodegenerative diseases such as Parkinson's illness, AIDS-associated dementia, Huntington's sickness, Down's syndrome, amyotrophic lateral sclerosis, and Alzheimer's disease as well as for the therapy of schizophrenia and myoclonus.^{31,32} In drug discovery, heterocyclic compounds comprising nitrogen have performed a very notable role. Due to the existence of heterocyclic compounds comprising a 2-pyrrolidinone core in natural products and their biological activity (Figure 2), they are one of the most important categories of heterocyclic compounds.³³ Many natural products such as thiomarinal A⁴, holomycin and thiolutin,³⁵ and lactacystin³⁶ contain a 2-pyrrolidinone scaffold (Figure 3). Especially, there is a wide range of pharmacological effects such as anti-tumor,³⁷ antibacterial, and anticonvulsant³⁸ in 2-pyrrolidinones. Therefore, the synthesis of 2-pyrrolidinones is another vital issue among chemists.

Given the interesting advantages of MCRs or recent developments in nanomaterial synthesis in catalysis science, herein, we reported for the first time the preparation of an efficient and recoverable novel magnetic Fe_3O_4 grafted sulfonic acid ($\text{SO}_3\text{H}/\text{NH}_2\text{NH}_2/\text{GPTMS}/\text{Fe}_3\text{O}_4$) and its application in the synthesis of pyran derivatives from dimedone, aldehydes derivatives, and malononitrile under reflux conditions in a 1:1 mixture of $\text{H}_2\text{O}/\text{EtOH}$, and the synthesis of substituted pyrrolidinones from aniline, aromatic aldehydes, and diethyl acetylenedicarboxylate in ethanol at a temperature of 50 °C in high yields (Scheme 1). We used a green catalyst and solvent, and mild reaction conditions for the one-pot synthesis of pyran and pyrrolidinone derivatives without generating harmful by-products. We found that no reference has been reported for the production of the various desired compounds in the presence of a green solvent, and magnetic Fe_3O_4 grafted sulfonic acid. Simple separation of products from the reaction mixture in high to excellent yields, low catalyst loading, good turnover frequency, and eco-friendliness are some astounding benefits of the present work.

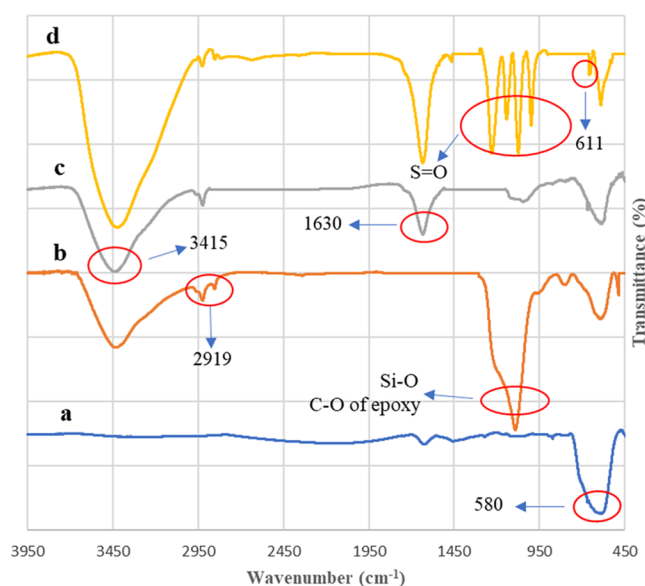
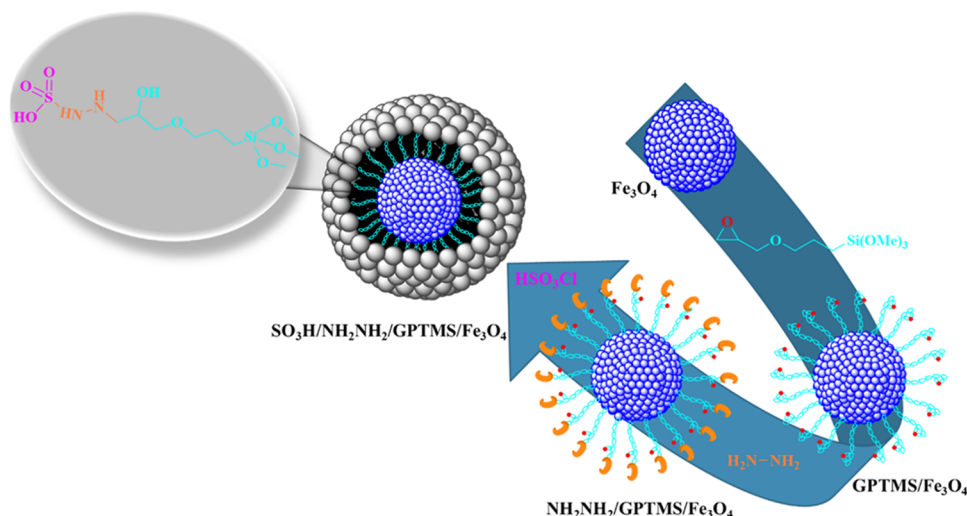
Scheme 1. Preparation of SO₃H/NH₂NH₂/GPTMS/Fe₃O₄ NPs

Figure 4. FT-IR spectra of (a) Fe₃O₄, (b) GPTMS/Fe₃O₄, (c) NH₂NH₂/GPTMS/Fe₃O₄, and (d) SO₃H/NH₂NH₂/GPTMS/Fe₃O₄.

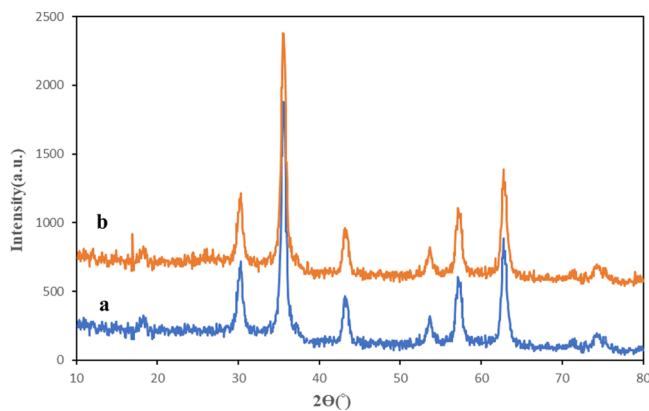


Figure 5. PXRD patterns of (a) Fe₃O₄ and (b) SO₃H/NH₂NH₂/GPTMS/Fe₃O₄.

Table 1. PXRD Data for SO₃H/NH₂NH₂/GPTMS/Fe₃O₄

| entry | 2θ (deg) | peak width (FWHM) | Miller indices | | | particle size (nm) | inter-planar distance (nm) |
|-------|----------|-------------------|----------------|----------|----------|--------------------|----------------------------|
| | | | <i>h</i> | <i>k</i> | <i>l</i> | | |
| 1 | 18.26 | 0.5904 | 1 | 1 | 1 | 13.6 | 0.485 |
| 2 | 30.37 | 0.4428 | 2 | 2 | 0 | 18.6 | 0.296 |
| 3 | 35.56 | 0.3444 | 3 | 1 | 1 | 24.2 | 0.253 |
| 4 | 43.19 | 0.6888 | 4 | 0 | 0 | 12.4 | 0.209 |
| 5 | 53.67 | 0.2952 | 4 | 2 | 2 | 30.2 | 0.171 |
| 6 | 57.29 | 0.7872 | 5 | 1 | 1 | 11.5 | 0.161 |
| 7 | 62.65 | 0.2952 | 4 | 4 | 0 | 31.5 | 0.148 |

2. EXPERIMENTAL SECTION

2.1. General. All materials containing iron (III) chloride, FeSO₄·7H₂O, aqueous ammonia (25%), ethanol, GPTMS, toluene (anhydrous), hydrazine hydrate, chlorosulfuric acid, benzaldehyde derivatives, dimedone, malononitrile, diethyl acetylenedicarboxylate, and aniline were provided from Fluka, Sigma-Aldrich, and Merck companies. FT-IR analyses were performed on a Perkin-Elmer 597 spectrophotometer. ¹H and ¹³C NMR spectra were acquired on a Bruker DRX-250 AVANCE spectrometer at 250 and 62.90 MHz, respectively. The crystallinity of the SO₃H/NH₂NH₂/GPTMS/Fe₃O₄ catalyst was surveyed using PXRD analysis (an X'Pert-Pro advanced diffractometer operated at 40 kV and 40 mA at 25 °C). EDAX was applied for elemental analysis of SO₃H/NH₂NH₂/GPTMS/Fe₃O₄ and achieved by applying an EDAX detector. SEM analysis was performed with a TE-SCAN (Brno, Czech Republic). Transmission electron microscopy (TEM) images were recorded on a Zeiss EM10C microscope, operated at 80 kV. VSM analysis was used to determine the magnetic properties of SO₃H/NH₂NH₂/GPTMS/Fe₃O₄ (VSM, Taban, Tehran, Iran).

2.2. Synthesis of Fe₃O₄ NPs. Fe₃O₄ magnetic nanoparticles were prepared by utilizing an improved chemical precipitation procedure.³⁹ First, FeSO₄·7H₂O and FeCl₃ (Fe²⁺/Fe³⁺ molar ratio = 1:2) were mixed in 120 mL of distilled H₂O at 80 °C. Next, 120 mL of a 25% aqueous solution of NH₃ (1.5 M) was added dropwise to the reaction mixture under a N₂ gas atmosphere. The obtained mixture was stirred in an N₂ gas atmosphere for 30 min. The reaction mixture was cooled to 25

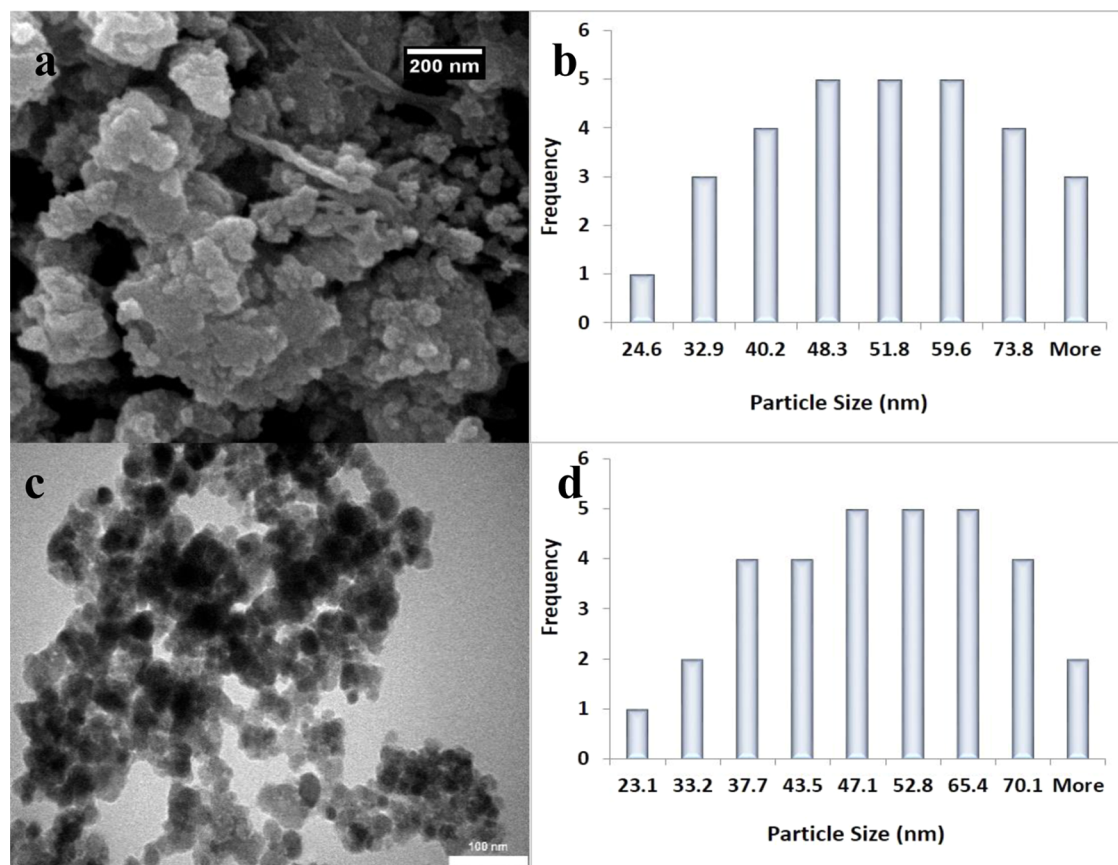


Figure 6. Microscopic analysis of $\text{SO}_3\text{H}/\text{NH}_2\text{NH}_2/\text{GPTMS}/\text{Fe}_3\text{O}_4$. (a) FE-SEM micrograph and (b) its size distribution diagram. (c) The TEM analysis and (d) its size distribution diagram.

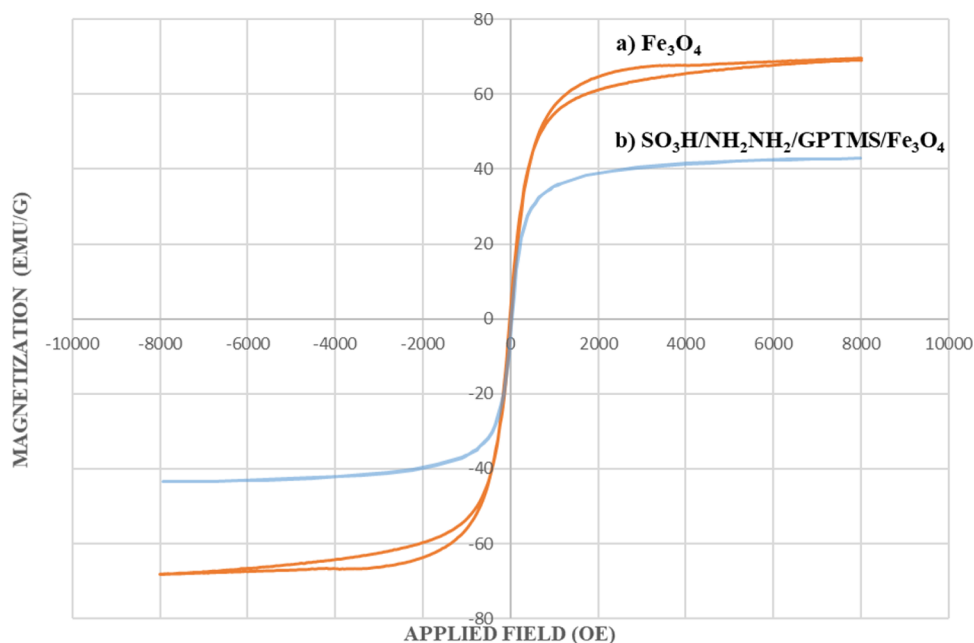


Figure 7. VSM analysis of (a) Fe_3O_4 and (b) $\text{SO}_3\text{H}/\text{NH}_2\text{NH}_2/\text{GPTMS}/\text{Fe}_3\text{O}_4$.

$^\circ\text{C}$, and the resulting black product was collected by using a simple magnet and eluted completely several times, first with distilled H_2O and then with EtOH. Fe_3O_4 magnetic nanoparticles were isolated and finally dried at 40°C for 24 h (yield: 92%).

2.3. Synthesis of $\text{GPTMS}/\text{Fe}_3\text{O}_4$. $\text{GPTMS}/\text{Fe}_3\text{O}_4$ was synthesized from GPTMS modified with Fe_3O_4 using an easy strategy.⁴⁰ Briefly, 1 g of Fe_3O_4 was suspended in 100 mL of anhydrous toluene for 20 min. Then, (3-glycidyoxypropyl)-trimethoxysilane (10 mmol) was added dropwise to the Fe_3O_4

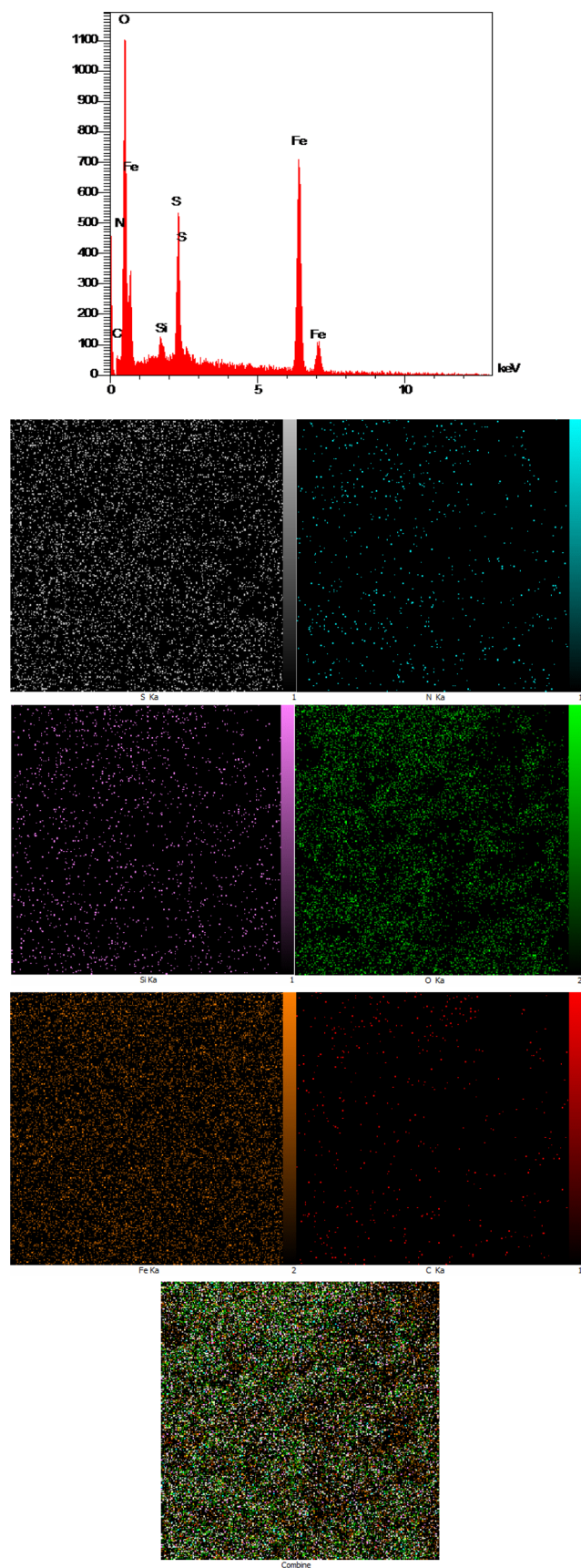


Figure 8. EDX and X-ray atomic mapping spectrum of SO_3H -functionalized epoxy-immobilized Fe_3O_4 core-shell MNPs.

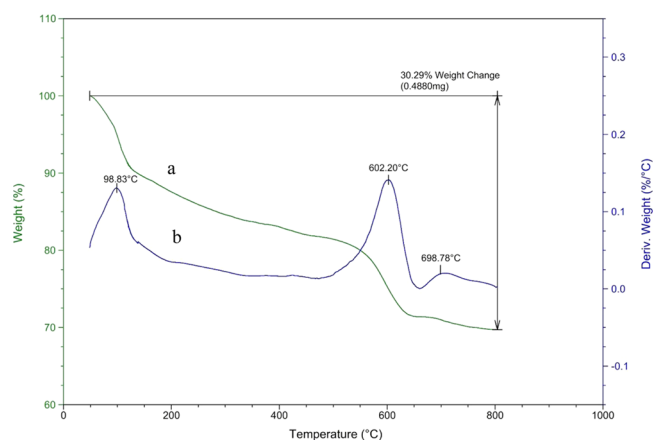


Figure 9. (a) Thermal gravimetric analysis (TGA) and (b) derivative thermal gravimetric (DTG) curves of $\text{SO}_3\text{H}/\text{NH}_2\text{NH}_2/\text{GPTMS}/\text{Fe}_3\text{O}_4$ NPs.

solution and was refluxed for 8 h under the protection of nitrogen. Finally, $\text{GPTMS}/\text{Fe}_3\text{O}_4$ was separated by applying a simple external magnet field and rinsed 2 times with benzene, and dried for 24 h at ambient temperature.

2.4. Synthesis of $\text{NH}_2\text{NH}_2/\text{GPTMS}/\text{Fe}_3\text{O}_4$. First, 1 g of $\text{GPTMS}/\text{Fe}_3\text{O}_4$ in 100 mL of dry toluene was suspended for 20 min. Next, hydrazine hydrate (12 mmol) was added to the $\text{GPTMS}/\text{Fe}_3\text{O}_4$ solution at reflux conditions under nitrogen gas for 24 h. Then, $\text{NH}_2\text{NH}_2/\text{GPTMS}/\text{Fe}_3\text{O}_4$ was separated by utilizing an external magnet, rinsed with benzene, and dried for 24 h at ambient temperature.

2.5. Synthesis of $\text{SO}_3\text{H}/\text{NH}_2\text{NH}_2/\text{GPTMS}/\text{Fe}_3\text{O}_4$. 1 g of $\text{NH}_2\text{NH}_2/\text{GPTMS}/\text{Fe}_3\text{O}_4$ NPs in 75 mL of dry CH_2Cl_2 were dispersed under ultrasound irradiation for 10 min. Afterward, 1 mL of ClSO_3H (15 mmol) was dissolved in 20 mL of CH_2Cl_2 and added dropwise to the $\text{NH}_2\text{NH}_2/\text{GPTMS}/\text{Fe}_3\text{O}_4$ stirring mixture over 30 min and the residual HCl was eventually eliminated by utilizing suction. Eventually, the obtained product was dried at 60°C (Scheme 1).⁴¹

2.6. General Procedure for the Synthesis of Pyrans (4a–n) by Using $\text{SO}_3\text{H}/\text{NH}_2\text{NH}_2/\text{GPTMS}/\text{Fe}_3\text{O}_4$. A mixture of aromatic aldehyde (1 mmol), malononitrile (1 mmol), and dimedone (1 mmol) for the synthesis of products (4a–n) containing $\text{SO}_3\text{H}/\text{NH}_2\text{NH}_2/\text{GPTMS}/\text{Fe}_3\text{O}_4$ (0.01 g) was stirred in 2 mL of $\text{EtOH}:\text{H}_2\text{O}$ (1:1) and refluxed for appropriate times. The reaction progress was investigated by utilizing TLC. Following the termination of the reaction, the nanocatalyst was eliminated from the reaction mixture by a simple external magnetic field, and then the precipitated product was recrystallized from ethanol.

2.7. General Procedure for the Preparation of Pyrrolidinones (7a–l) by Utilizing $\text{SO}_3\text{H}/\text{NH}_2\text{NH}_2/\text{GPTMS}/\text{Fe}_3\text{O}_4$. A mixture of aromatic aldehyde (1 mmol), aniline (1 mmol), diethyl acetylenedicarboxylate (1 mmol), and $\text{SO}_3\text{H}/\text{NH}_2\text{NH}_2/\text{GPTMS}/\text{Fe}_3\text{O}_4$ (0.015 g) in EtOH (2 mL) was stirred at 60°C . TLC was applied to follow the reaction, then the obtained products were heated in EtOH until dissolved. After removing the nanocatalyst from the reaction mixture by employing a simple magnet, the pure products were prepared through recrystallization from hot EtOH .

2.8. FT-IR and NMR Spectral Data of Some Products.

2.8.1. 2-Amino-7,7-dimethyl-4-(4-chlorophenyl)-5-oxo-5,6,7,8-tetrahydrobenzo[b]pyran (4a). FT-IR (KBr): 3380, 3182, 2958, 2188, 1675, 1604, 1491, 1418, 1364, 1246, 1216,

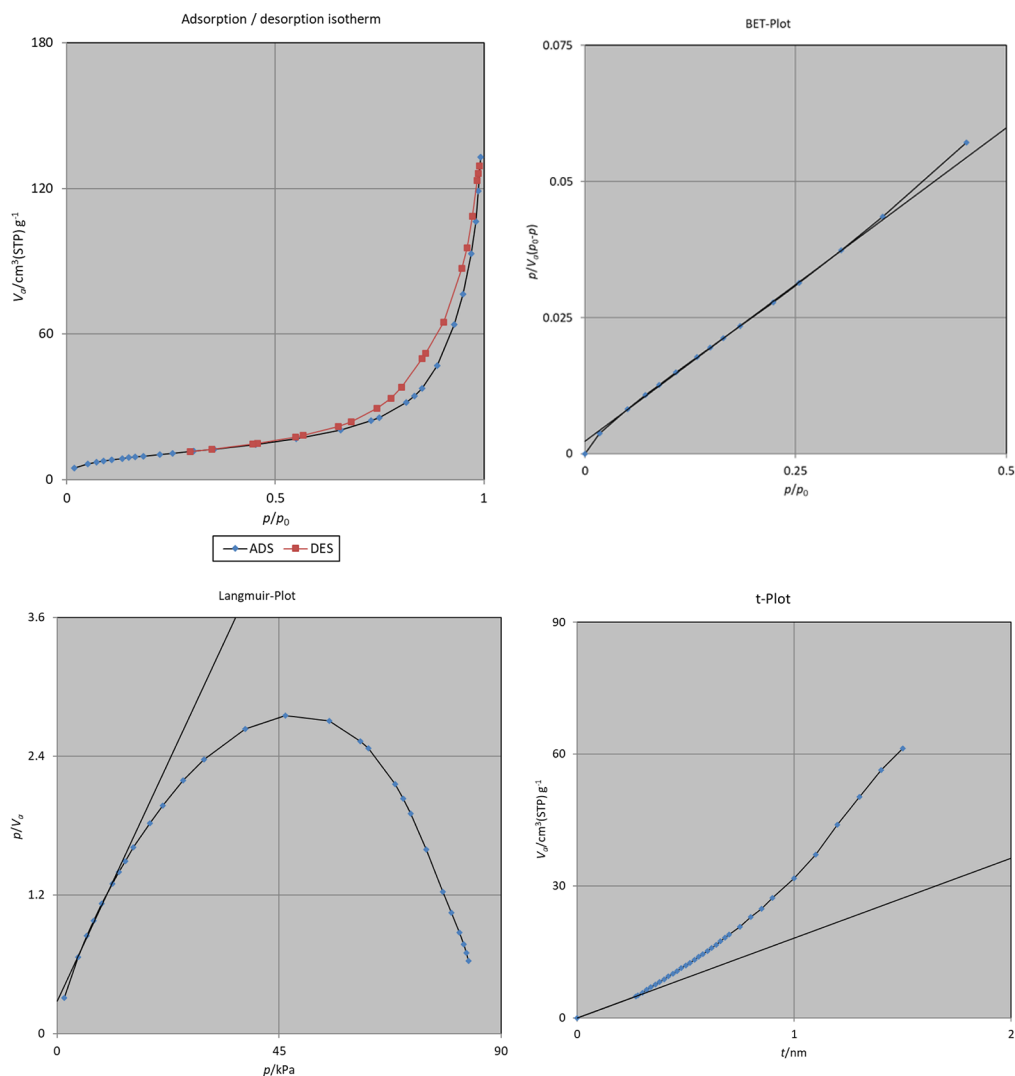


Figure 10. BET plot of the N₂ adsorption–desorption and BET plot of N₂ adsorption isotherms of SO₃H/NH₂NH₂/GPTMS/Fe₃O₄.

1140, 1094, 1032, 1014, 854, 770. ¹H NMR (250.13 MHz, DMSO-*d*₆) δ_H = 0.92 (s, 3H, CH₃), 1.00 (s, 3H, CH₃), 2.07 (d, *J* = 15.7, 1H, CH₂), 2.22 (d, *J* = 15.7, 1H, CH₂), 2.48 (br, 2H, CH₂), 4.16 (s, 1H, CH), 7.03–7.33 (m, 6H, 4CH_{Ar}, NH₂). ¹³C NMR (62.90 MHz, DMSO-*d*₆): δ = 22.8, 24.2, 27.7, 31.1, 36.1, 45.9, 53.7, 108.3, 115.5, 124.2, 125.1, 127.1, 139.7, 154.4, 158.6, 191.6.

2.8.2. 2-Amino-7,7-dimethyl-4-(4-bromophenyl)-5-oxo-5,6,7,8-tetrahydrobenzo[b]pyran (4b). FT-IR (KBr): 3399, 3323, 2964, 2191, 1686, 1605, 1486, 1406, 1362, 1254, 1217, 1160, 1038, 845, 562. ¹H NMR (250.13 MHz, DMSO-*d*₆) δ_H = 0.95 (s, 3H, CH₃), 1.09 (s, 3H, CH₃), 2.08–2.17 (m, 2H, CH₂), 2.46 (br, 2H, CH₂), 4.13 (s, 1H, CH), 7.04–7.43 (m, 6H, 4CH_{Ar}, NH₂). ¹³C NMR (62.90 MHz, DMSO-*d*₆): δ = 23.9, 24.2, 27.7, 34.8, 36.1, 45.9, 56.7, 108.2, 115.5, 124.6, 125.4, 127.1, 140.1, 154.4, 158.5, 191.6.

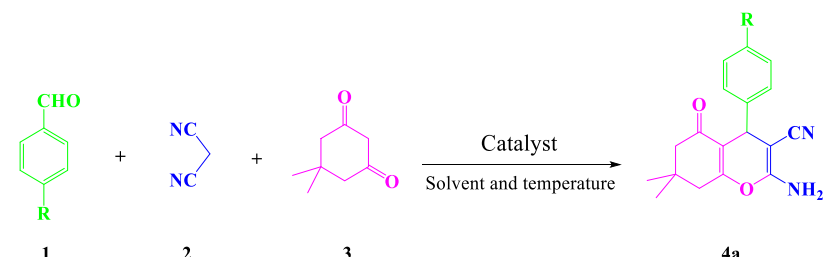
2.8.3. 2-Amino-7,7-dimethyl-4-(4-cyanophenyl)-5-oxo-5,6,7,8-tetrahydrobenzo[b]pyran (4c). FT-IR (KBr): 3353, 2962, 2228, 2193, 1690, 1604, 1503, 1362, 1253, 1215, 1039, 859. ¹H NMR (250.13 MHz, DMSO-*d*₆) δ_H = 0.92 (s, 3H, CH₃), 1.00 (s, 3H, CH₃), 2.07 (d, *J* = 15.5, 1H, CH₂), 2.22 (d, *J* = 14.2, 1H, CH₂), 2.49 (br, 2H, CH₂), 4.26 (s, 1H, CH), 7.12 (s, 2H, NH₂), 7.33 (d, *J* = 7.5 Hz, 2H, CH_{Ar}), 7.73 (d, *J* = 7.2 Hz, 2H, CH_{Ar}). ¹³C NMR (62.90 MHz, DMSO-*d*₆): δ = 22.8, 24.1,

27.7, 31.7, 35.0, 45.7, 53.0, 105.3, 107.6, 114.6, 115.2, 124.2, 128.3, 146.1, 154.5, 159.0, 191.6.

2.8.4. Ethyl 2-(4-Chlorophenyl)-4-hydroxy-5-oxo-1-phenyl-2,5-dihydro-1H-pyrrole-3-carboxylate (7a). FT-IR (KBr): 3287, 2960, 1721, 1683, 1652, 1369, 1258, 1216, 1190, 1035, 687. ¹H NMR (250.13 MHz, DMSO-*d*₆) δ_H = 1.01 (t, 3H, CH₃), 3.97 (q, 2H, CH₂), 6.41 (s, 1H, CH), 7.14–7.72 (m, 9H, CH_{Ar}), 11.64 (br s, 1H, OH). ¹³C NMR (62.90 MHz, DMSO-*d*₆): δ = 9.9, 55.7, 107.7, 118.5, 121.4, 124.2, 125.7, 128.5, 131.7, 132.0, 148.8, 159.7.

2.8.5. Ethyl 2-(2-Chlorophenyl)-4-hydroxy-5-oxo-1-phenyl-2,5-dihydro-1H-pyrrole-3-carboxylate (7b). FT-IR (KBr): 3300, 2986, 1728, 1499, 1076. ¹H NMR (250.13 MHz, DMSO-*d*₆) δ_H = 1.01 (t, 3H, CH₃), 3.97 (q, 2H, CH₂), 6.41 (s, 1H, CH), 7.14–7.72 (m, 9H, CH_{Ar}), 11.84 (1H, OH). ¹³C NMR (62.90 MHz, DMSO-*d*₆): δ = 9.8, 52.6, 57.9, 107.8, 118.4, 122.2, 123.4, 124.8, 125.6, 126.9, 130.3, 131.5, 132.1, 149.6, 157.7, 160.1.

2.8.6. Ethyl 2-(4-Fluorophenyl)-4-hydroxy-5-oxo-1-phenyl-2,5-dihydro-1H-pyrrole-3-carboxylate (7c). FT-IR (KBr): 3295, 2984, 2926, 1717, 1498, 1026. ¹H NMR (250.13 MHz, DMSO-*d*₆) δ_H = 1.06 (s, 3H, CH₃), 4.02 (s, 2H, CH₂), 6.06 (s, 1H, CH), 7.02–7.53 (m, 9H, CH_{Ar}), 11.73 (1H, OH). ¹³C NMR (62.90 MHz, DMSO-*d*₆): δ = 10.0, 55.7, 107.9, 110.9, 111.2,

Table 2. Optimizing the Catalyst Amount, Solvent, and Temperature According to the Model Reaction for the Preparation of 4a^a


| entry | catalyst (g) | solvent | temperature (°C) | time (min) | yield (%) ^b |
|-------|--------------|---------------------------------|------------------|------------|------------------------|
| 1 | | | | 120 | trace |
| 2 | | H ₂ O/EtOH (1:1) | reflux | 120 | 10 |
| 3 | 0.005 | EtOH | r.t. | 150 | 50 |
| 4 | 0.005 | H ₂ O | r.t. | 260 | 45 |
| 5 | 0.005 | CH ₃ CN | r.t. | 260 | 28 |
| 6 | 0.005 | DMF | r.t. | 260 | 25 |
| 7 | 0.005 | CH ₂ Cl ₂ | r.t. | 300 | 35 |
| 8 | 0.005 | ethyl acetate | r.t. | 300 | 30 |
| 9 | 0.005 | toluene | r.t. | 300 | 15 |
| 10 | 0.005 | H ₂ O/EtOH (1:1) | r.t. | 150 | 78 |
| 11 | 0.01 | H ₂ O/EtOH (1:1) | r.t. | 90 | 83 |
| 12 | 0.02 | H ₂ O/EtOH (1:1) | r.t. | 50 | 70 |
| 13 | 0.005 | H ₂ O/EtOH (1:1) | 70 | 90 | 82 |
| 14 | 0.01 | H ₂ O/EtOH (1:1) | 70 | 35 | 88 |
| 15 | 0.02 | H ₂ O/EtOH (1:1) | 70 | 60 | 78 |
| 16 | 0.005 | H ₂ O/EtOH (1:1) | reflux | 35 | 87 |
| 17 | 0.01 | H ₂ O/EtOH (1:1) | reflux | 15 | 95 |
| 18 | 0.02 | H ₂ O/EtOH (1:1) | reflux | 15 | 90 |

^aReaction conditions: 4-chlorobenzaldehyde (1 mmol), malononitrile (1 mmol), and dimedone (1 mmol), solvent (2 mL), and catalyst. ^bIsolated yield.

Table 3. Comparison of the Activity of Different Catalysts in the Preparation of 4a^a

| entry | catalyst | condition | time (min) | yield (%) ^b |
|-------|---|-------------------------------|------------|------------------------|
| 1 | | H ₂ O/EtOH, reflux | 120 | 25 |
| 2 | H ₂ SO ₄ | H ₂ O/EtOH, reflux | 20 | 65 |
| 3 | HSO ₄ Cl | H ₂ O/EtOH, reflux | 120 | |
| 4 | SO ₃ H/NH ₂ NH ₂ /GPTMS | H ₂ O/EtOH, reflux | 45 | 65 |
| 5 | Fe ₃ O ₄ | H ₂ O/EtOH, reflux | 60 | 48 |
| 6 | FeCl ₃ | H ₂ O/EtOH, reflux | 60 | 52 |
| 7 | FeSO ₄ ·7H ₂ O | H ₂ O/EtOH, reflux | 90 | 45 |
| 8 | GPTMS/Fe ₃ O ₄ | H ₂ O/EtOH, reflux | 60 | 23 |
| 9 | NH ₂ NH ₂ /GPTMS/Fe ₃ O ₄ | H ₂ O/EtOH, reflux | 50 | 79 |
| 10 | SO ₃ H/NH ₂ NH ₂ /GPTMS/Fe ₃ O ₄ | H ₂ O/EtOH, reflux | 15 | 95 |

^aReaction conditions: 4-chlorobenzaldehyde (1 mmol), malononitrile (1 mmol), and dimedone (1 mmol), solvent (2 mL), and catalyst (0.01 g), under reflux. ^bIsolated yield.

118.6, 121.4, 124.7, 125.9, 128.8, 132.1, 148.8, 155.6, 157.9, 159.9.

2.9. X-ray Crystallography. Crystallographic measurements of 7a and 7d were carried out on a κ -geometry Agilent

Technologies Xcalibur R four-circle diffractometer (ω scans) with Mo K α radiation ($\lambda = 0.71073$ Å) and a Ruby CCD detector at 100(2) K. The collected data were corrected for the Lorentz and polarization effects. Data collection, cell refinement, data reduction, and analysis, including empirical (multi-scan) absorption correction, were performed with *CrysAlisPRO*.⁴² Structures were solved using SHELXT-2014⁴³ and refined by a full-matrix least-squares technique with the anisotropic displacement parameters for non-H atoms with the use of SHELXL-2014.⁴⁴ The structure of 7a was refined as a two-component twin. The H atoms in both structures were found in difference Fourier maps or were included from geometrical considerations, and were initially refined isotropically. In the final refinement cycles, the C-bonded H atoms in both 7a and 7d, and hydroxyl H atoms in 7a were repositioned in their computed positions and refined using a riding model, with C–H = 0.95–1.00 Å, O–H = 0.84, and $U_{\text{iso}}(\text{H}) = 1.2U_{\text{eq}}(\text{C})$ for CH and CH₂, and $1.5U_{\text{eq}}(\text{C}, \text{O})$ for CH₃ and OH. A hydrogen atom of the hydroxyl group in 7d was refined freely. Labels of atoms in both structures have been adjusted to the structure deposited at the Cambridge Structural Database (CSD, Version 5.40)⁴⁵ with the CSD refcode LIFBEJ.⁴⁶ The XP and Diamond programs were used to create the figures.^{47,48} Details of structures refinement and crystals data can be found in Table S1 as well as in the crystallographic information files (CIF) deposited at the Cambridge Crystallographic Data Centre (CCDC No. 2215544 and 2215545).

Table 4. Preparation of 4H-Pyran Derivatives^{51–57} Catalyzed by SO₃H/NH₂NH₂/GPTMS/Fe₃O₄^a

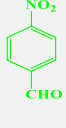
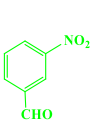
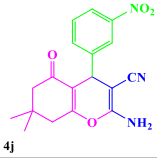
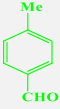
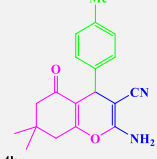
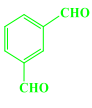
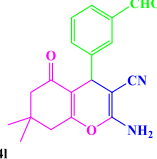
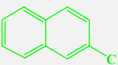
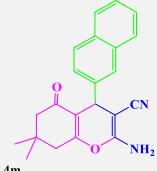
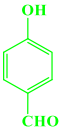
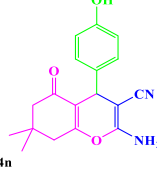
| Entry | Aldehyde | Products (4a-n) | Time (min) | Yield (%) ^b | M.P. (°C) | M.P. (°C) (Ref.) |
|-------|---|---|------------|------------------------|-----------|-----------------------|
| 1 |  |  4a | 15 | 95 | 215-217 | 215-217 ⁵¹ |
| 2 |  |  4b | 20 | 95 | 220-222 | 221-223 ⁵² |
| 3 |  |  4c | 10 | 96 | 226-228 | 225-228 ⁵³ |
| 4 |  |  4d | 20 | 93 | 197-201 | 198-202 ⁵⁴ |
| 5 |  |  4e | 15 | 93 | 233-235 | 233-235 ⁵⁴ |
| 6 |  |  4f | 15 | 95 | 188-189 | 187-188 ⁵² |
| 7 |  |  4g | 20 | 76 | 155-156 | 154-156 ⁵² |
| 8 |  |  4h | 17 | 82 | 175-177 | 174-177 |
| 9 |  |  4i | 10 | 96 | 179-181 | 178-180 ⁵⁴ |

Table 4. continued

| Entry | Aldehyde | Products (4a-n) | Time (min) | Yield (%) ^b | M.P. (°C) | M.P. (°C) (Ref.) |
|-------|--|--|------------|------------------------|-----------|-----------------------|
| 10 |  |  4j | 15 | 96 | 205-207 | 206-208 ⁵⁵ |
| 11 |  |  4k | 20 | 92 | 220-222 | 223-225 ⁵⁶ |
| 12 |  |  4l | 25 | 89 | 202-204 | 203-205 ⁵² |
| 13 |  |  4m | 15 | 86 | 230-231 | 229-231 ⁵⁵ |
| 14 |  |  4n | 20 | 86 | 225-227 | 224-226 ⁵⁷ |

^aReaction conditions: aromatic aldehyde (1 mmol), malononitrile (1 mmol), and dimedone (1 mmol), H₂O:EtOH (2 mL), and catalyst (0.01 g), under reflux. ^bIsolated yield.

3. RESULTS AND DISCUSSION

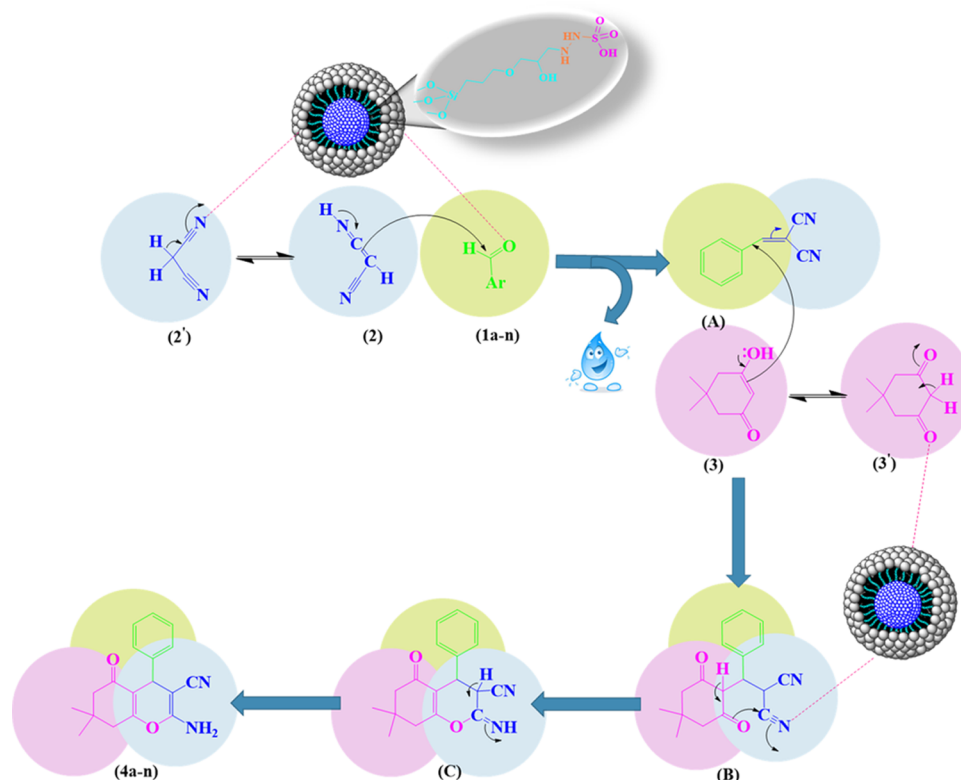
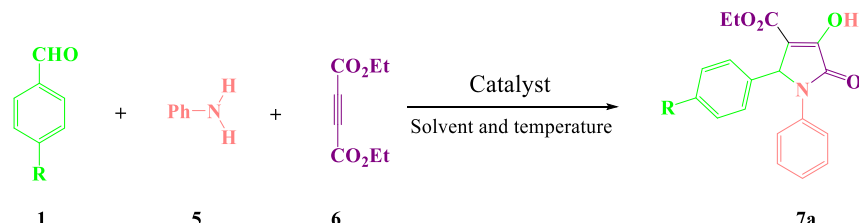
Magnetic Fe₃O₄ grafted sulfonic acid (SO₃H/NH₂NH₂/GPTMS/Fe₃O₄) was successfully prepared in an operationally simple procedure in three steps (Scheme 1). First, epoxy-functionalized Fe₃O₄ core-shell MNP (GPTMS/Fe₃O₄) was obtained through grafting Fe₃O₄ NPs with GPTMS and subsequently, epoxy-attached Fe₃O₄ core-shell MNP were immobilized with hydrazine and finally, chlorosulfonic acid was immobilized on NH₂NH₂/GPTMS/Fe₃O₄ core-shell MNPs by employing a dropwise approach. The nanostructured magnetic catalyst was identified by utilizing Fourier transform infrared (FT-IR) spectroscopy, Brunauer–Emmet–Teller (BET) analysis, field emission scanning electron microscopy (FE-SEM), energy-dispersive X-ray analysis (EDX), vibrating sample magnetometry (VSM), thermogravimetric analysis (TGA), and powder X-ray diffraction (PXRD).

The FT-IR technique was utilized to detect diverse functional groups of Fe₃O₄@GP@NH₂NH₂@SO₃H step by step (Figure 4). The FT-IR spectra of (a) Fe₃O₄, (b) GPTMS/Fe₃O₄, (c) NH₂NH₂/GPTMS/Fe₃O₄, and (d) SO₃H/NH₂NH₂/GPTMS/Fe₃O₄ are illustrated in Figure 4. Figure 4a–d shows the strong vibration band related to the Fe–O group at 580 cm⁻¹. The wide peaks at 1089–1186 cm⁻¹ were assigned to Si–O and the epoxy groups of (3-glycidyloxypropyl)trimethoxysilane (GPTMS) as depicted in Figure 4b–d. Also, the alkyl CH₂ stretching vibration appeared at 2919 cm⁻¹ (Figure 4b–d). A broad

absorption peak at 3415 cm⁻¹ appeared belonging to the NH and OH groups. N–H bending vibration of hydrazine appears at 1630 cm⁻¹ (Figure 4b–d). The appearance of a new peak at 1000–1350 cm⁻¹ can be assigned to the stretching vibration peak of S=O bonds. Also, the C–S band at 611 cm⁻¹ was observed in Figure 4d. These data emphasize the successful coating of chlorosulfonic acid moieties onto the NH₂NH₂/GPTMS/Fe₃O₄ surface.

The PXRD patterns of the Fe₃O₄ and SO₃H/NH₂NH₂/GPTMS/Fe₃O₄ are depicted in Figure 5. The strong and sharp diffraction peaks of the synthesized nanocatalyst at 2θ = 18.26, 30.37, 35.56, 43.19, 53.67, 57.29, and 62.65° associated with the various planes such as the (111), (220), (311), (400), (422), (511), and (440) were readily specified from the PXRD pattern of cubic Fe₃O₄ (JCPDS 88-0866).⁴⁹ PXRD analysis confirms the successful preparation of the designed nanocatalyst with the sameness of the pure phase pattern of SO₃H/NH₂NH₂/GPTMS/Fe₃O₄ with the Fe₃O₄ pattern. Also, the Miller indices, peak width (FWHM), inter-planar distance, and size of SO₃H/NH₂NH₂/GPTMS/Fe₃O₄ in the 18.26–62.65 range were calculated and the obtained results are represented in Table 1. The average crystallite size and inter-planar distance were respectively determined at 20.28 and 0.246 nm through the Scherrer equation [$D = K\lambda/(\beta \cos \Theta)$] and Bragg equation [$d_{hkl} = \lambda/(2 \sin \Theta)$].

Scheme 2. Suggested Mechanism for the Formation of 4H-Pyran Derivatives

Table 5. Effect of the Catalyst Amount, Solvent, and Temperature on the Preparation of 4a^a

| entry | catalyst (g) | solvent | temperature (°C) | time (min) | yield (%) ^b |
|-------|--------------|---------------------------------|------------------|------------|------------------------|
| 1 | | EtOH | 50 | 54 | |
| 2 | 0.005 | EtOH | 50 | 18 | 61 |
| 3 | 0.01 | EtOH | 50 | 15 | 80 |
| 4 | 0.015 | EtOH | 50 | 15 | 93 |
| 5 | 0.02 | EtOH | 50 | 15 | 86 |
| 6 | 0.015 | EtOH | r.t. | 36 | trace |
| 7 | 0.015 | EtOH | reflux | 18 | 78 |
| 8 | 0.015 | H ₂ O/EtOH (1:1) | reflux | 18 | 67 |
| 9 | 0.015 | H ₂ O | reflux | 18 | 35 |
| 10 | 0.015 | CH ₃ CN | reflux | 36 | 69 |
| 11 | 0.015 | | 50 | 36 | 49 |
| 12 | 0.015 | CH ₂ Cl ₂ | reflux | 36 | 67 |
| 13 | 0.015 | CH ₃ OH | reflux | 36 | 75 |
| 14 | 0.015 | ethyl acetate | reflux | 36 | 65 |

^aReaction conditions: 4-chlorobenzaldehyde (1 mmol), aniline (1 mmol) and diethyl acetylenedicarboxylate (1 mmol), solvent (2 mL), and catalyst. ^bIsolated yield.

FE-SEM images (Figure 6a,b) specified the structural features, morphologies, and particle size of SO₃H/NH₂NH₂/GPTMS/Fe₃O₄. Actually, FE-SEM analysis shows a uniform size distribution diagram with an average size of 48–59 nm (Figure 6b). TEM imaging of SO₃H/NH₂NH₂/GPTMS/Fe₃O₄ illustrates the core–shell structure (Figure 6c) with the uniform

size distribution diagram with an average size of 47–65 nm (Figure 6d).

The magnetic characteristics of (a) Fe₃O₄ and (b) SO₃H/NH₂NH₂/GPTMS/Fe₃O₄ were identified through VSM at 25 °C (Figure 7). For the Fe₃O₄, the saturation magnetization value was obtained as 69.8 emu·g⁻¹. The magnetization value of

Table 6. Comparison of the Activity of Different Catalysts in the Preparation of 7a^a

| entry | catalyst | conditions | time (min) | yield (%) ^b |
|-------|---|----------------|------------|------------------------|
| 1 | H ₂ SO ₄ | EtOH, 50 °C | 145 | |
| 2 | HSO ₄ Cl | EtOH, 50 °C | 145 | |
| 3 | SO ₃ H/NH ₂ NH ₂ /GPTMS | EtOH, 50 °C | 20 | 58 |
| 4 | Fe ₃ O ₄ | EtOH, 50 °C | 145 | |
| 5 | FeCl ₃ | EtOH, 50 °C | 145 | |
| 6 | FeSO ₄ ·7H ₂ O | EtOH, 50 °C | 145 | |
| 7 | GPTMS/Fe ₃ O ₄ | EtOH, 50 °C | 145 | |
| 8 | NH ₂ NH ₂ /GPTMS/Fe ₃ O ₄ | EtOH, 50 °C | 145 | |
| 9 | SO ₃ H/NH ₂ NH ₂ /GPTMS/Fe ₃ O ₄ | EtOH, 50 °C | 15 | 93 |

^aReaction conditions: 4-chlorobenzaldehyde (1 mmol), aniline (1 mmol) and diethyl acetylenedicarboxylate (1 mmol), solvent (2 mL), and catalyst (0.015 g), 50 °C. ^bIsolated yield.

SO₃H/NH₂NH₂/GPTMS/Fe₃O₄ was 45 emu·g⁻¹, which was lower than that of the Fe₃O₄ NPs. These results represented that the magnetization of Fe₃O₄ NPs decreased after the modification process with silica layers and organic compounds.

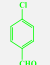
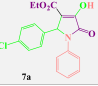
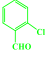
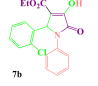
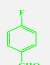
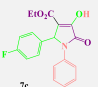
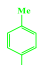
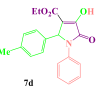
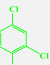
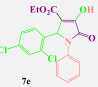
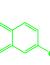
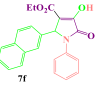
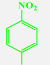
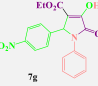
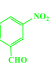
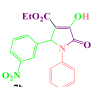
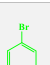
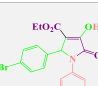
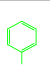
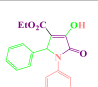
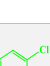
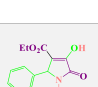
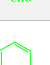
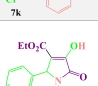
The EDX image was applied for obtaining information about the elemental distribution in the SO₃H/NH₂NH₂/GPTMS/Fe₃O₄ structure (Figure 8). In the case of SO₃H/NH₂NH₂/GPTMS/Fe₃O₄, coating functional groups onto the surface of MNPs was confirmed by the presence of C, Fe, O, S, Si, and N signals (Figure 8). It could be concluded that the designed nanocatalyst has been successfully prepared. Also, the presence of C, Fe, O, S, Si, and N elements was exhibited by the elemental map of the SO₃H/NH₂NH₂/GPTMS/Fe₃O₄ nanocatalyst (Figure 8).

As shown in Figure 9, TGA analysis was performed in the 25–800 °C range (Figure 9). The first weight loss of about 4% for SO₃H/NH₂NH₂/GPTMS/Fe₃O₄ at 98.83 °C corresponds to H₂O and physically adsorbed solvents. The second mass reduction of about 17% occurred for the catalyst at ~602 °C, which can be related to the demolition of diverse organic compounds immobilized onto the surface of Fe₃O₄ NPs. Also, the third mass reduction observed at nearly 698 °C is a result of the elimination of the silanol groups, which explains the weight loss of about 30.29%.

BET analysis was performed to know the mean pore diameter, total pore volume, surface area, and type of isotherm of SO₃H/NH₂NH₂/GPTMS/Fe₃O₄. Figure 10 shows the BET plot of the N₂ adsorption–desorption and BET plot of N₂ adsorption isotherm images. As can be seen, the total pore volume, surface area, and the mean pore diameter of SO₃H/NH₂NH₂/GPTMS/Fe₃O₄ were 0.1842 cm³ g⁻¹, 35.451 m² g⁻¹, and 23.156 nm, respectively. Also, the synthesized nanocatalyst is categorized as type IV isotherm, which belongs to the mesoporous range.⁵⁰

After the determination of the survey structure of SO₃H-functionalized epoxy-immobilized Fe₃O₄ core–shell MNP, its catalytic efficiency was evaluated in the preparation of tetrahydrobenzo[*b*]pyran and 3-pyrrolin-2-one derivatives (Scheme 1).

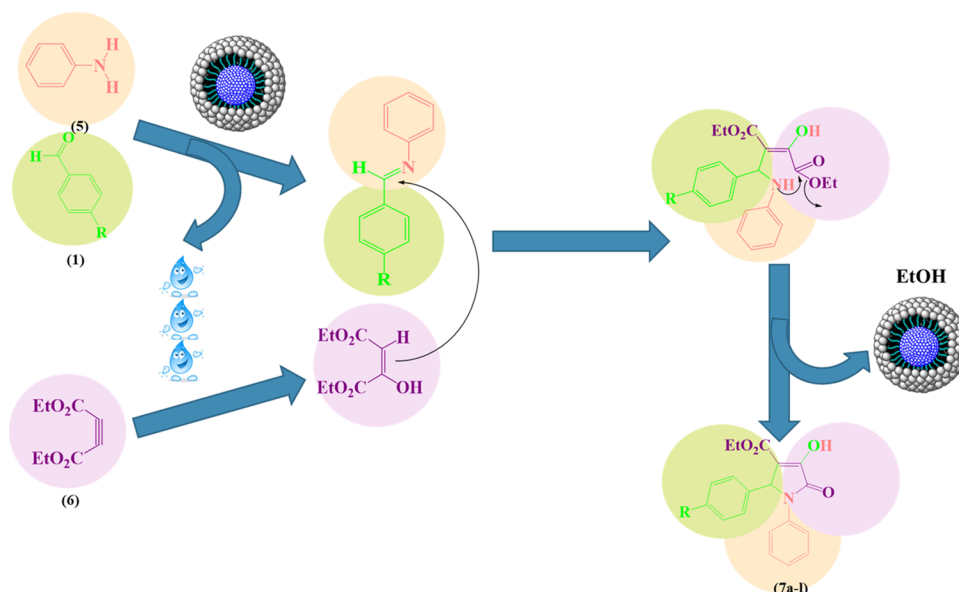
Table 7. Preparation of 3-Pyrrolin-2-One Derivatives by Employing SO₃H/NH₂NH₂/GPTMS/Fe₃O₄^a 58,59

| Entry | Aldehyde | Products (7a-l) | Time (min) | Yield (%) ^b | M.P. (°C) | M.P. (°C) (Ref.) |
|-------|---|---|------------|------------------------|-----------|-----------------------|
| 1 |  |  | 15 | 93 | 194-197 | 195-198 ²⁷ |
| 2 |  |  | 20 | 92 | 205-206 | 204-207 ²⁷ |
| 3 |  |  | 15 | 92 | 192-195 | 193-196 ²⁷ |
| 4 |  |  | 15 | 87 | 200-203 | 202-205 ²⁷ |
| 5 |  |  | 15 | 91 | 210-211 | 211-213 ⁵⁸ |
| 6 |  |  | 20 | 87 | 224-226 | 225-228 ²⁷ |
| 7 |  |  | 20 | 90 | 180-183 | 181-183 ⁵⁹ |
| 8 |  |  | 20 | 91 | 224-226 | 225-227 ⁶⁰ |
| 9 |  |  | 20 | 92 | 190-193 | 190-192 ⁶¹ |
| 10 |  |  | 15 | 88 | 179-181 | 178-180 ⁶² |
| 11 |  |  | 20 | 92 | 183-185 | 184-187 ⁶⁰ |
| 12 |  |  | 15 | 91 | 203-204 | 202-205 ⁶¹ |

^aReaction conditions: aromatic aldehyde (1 mmol), aniline (1 mmol) and diethyl acetylenedicarboxylate (1 mmol), EtOH (2 mL), and catalyst (0.015), 50 °C. ^bIsolated yield.

To optimize the synthesis of pyrans, the effect of different parameters, for instance, solvents, amounts of the catalyst, and temperature in the reaction of malononitrile with 4-chlorobenzaldehyde and dimedone as a model reaction were tested (Table 2). Reaction performance with different solvents, including EtOH, H₂O, CH₃CN, DMF, CH₂Cl₂, ethyl acetate, toluene, and H₂O/EtOH (1:1) was performed to explore the solvent effect (Table 2, entries 3–10). As shown in Table 2, good yield (78%) was obtained in a short reaction time (150

Scheme 3. Proposed Mechanistic Path for the Preparation of Substituted 3-Pyrrolin-2-Ones



min) for 1:1 H₂O/EtOH compared with other solvents listed in the table in the presence of 0.005 g of the catalyst at room temperature (Table 2, entry 10). The results in Table 2 illustrate that the reaction is sensitive to temperature. Importantly, upon increasing the temperature, a decrease in the time and an increase in the reaction yield are observed (Table 2, entries 13–18). In our study, the effect of the catalyst amount was also perused based on the model reaction at 0.005, 0.01, and 0.02 g to discern their efficiency at 70 °C temperature and reflux conditions (Table 2, entries 13–18). Among the tested amounts, 0.01 g of the catalyst under reflux conditions was selected as the optimal amount and conditions in a 1:1 mixture of H₂O/EtOH (Table 2, entry 17). When the reaction was performed by employing 0.01 g of the catalyst under reflux conditions in a 1:1 mixture of H₂O/EtOH, the best product yield in a very shorter time of condensation of malononitrile with 4-chlorobenzaldehyde and dimedone was acquired (Table 2, entry 17).

Table 3 shows higher activity of the SO₃H/NH₂NH₂/GPTMS/Fe₃O₄ catalyst, for instance, the loading catalyst, reaction time, and yield rather than other catalysts to synthesize product 4a. When H₂SO₄ (Table 3, entry 2), SO₃H/NH₂NH₂/GPTMS (Table 3, entry 4), Fe₃O₄ (Table 3, entry 5), FeCl₃ (Table 3, entry 6), and FeSO₄·7H₂O (Table 3, entry 7) were applied as the catalyst, a moderate yield was acquired for product 4a., although a decreased yield (23%) and a no yield was observed when GPTMS/Fe₃O₄ and HSO₄Cl was utilized, respectively (Table 3, entry 8). When NH₂NH₂/GPTMS/Fe₃O₄ was utilized, the desired product 4a was obtained with 79% yield (Table 3, entry 9).

Preparation of 4H-pyran derivatives was investigated by utilizing a series of aromatic aldehydes with malononitrile and dimedone under optimum conditions to evaluate the generality, limitation, and applicability of this method. As shown in Table 4, all aromatic aldehydes including aldehydes with electron-donating substitutions such as 4-HO-benzaldehyde, 4-MeO-benzaldehyde, 4-Me-benzaldehyde, and electron-withdrawing substitutions containing aldehydes such as 4-NO₂-benzaldehyde, and 4-CN-benzaldehyde have led to the synthesis of the

corresponding tetrahydrobenzo[*b*]pyrans in high to excellent yields and no side products have been observed.

The suggested mechanism for the synthesis of 4H-pyran derivatives commences with the protonation of aldehyde and malononitrile and is shown in Scheme 2. First, intermediate A is formed from the reaction between malononitrile and aromatic aldehyde. Subsequently, E1cB elimination of water from intermediate A is facilitated by utilizing the SO₃H/NH₂NH₂/GPTMS/Fe₃O₄ catalyst. Then, dimedone is converted to an enolized form in the presence of a catalyst and attacks intermediate A for forming intermediate B. In the next step, intermediate C is afforded after intramolecular cyclization. Finally, the pyran product is formed from intermediate C by employing a hydrogen shift (Scheme 2).

In another study to investigate the catalytic activity of SO₃H/NH₂NH₂/GPTMS/Fe₃O₄ in the formation of 3-pyrrolin-2-ones derivatives, the reaction of 4-chlorobenzaldehyde 1 (1 mmol), aniline 5 (1 mmol), and diethyl acetylenedicarboxylate 6 (1 mmol) was chosen as a model reaction. Optimization of the reaction conditions was done in terms of temperature, solvent, catalyst amount, time, and yield. Table 5 represents that the reaction without SO₃H/NH₂NH₂/GPTMS/Fe₃O₄ and without the desired product was carried out for 54 min (Table 5, entry 1). The effect of the amount of nanocatalyst (0.005–0.02 g) on the model reaction was surveyed (Table 5, entries 2–5). Excellent yield (93%) and short reaction time (15 min) were acquired in 0.015 g of SO₃H/NH₂NH₂/GPTMS/Fe₃O₄ in EtOH at 50 °C (Table 5, entry 4). Then, the amount of the nanocatalyst from 0.01 to 0.015 g, and 0.02 g was increased as the reaction yield and reaction time were not appropriate (Table 5, entries 3–5). As shown in Table 5, it is clear from entry 6 that the reaction with 0.015 g of the nanocatalyst at 50 °C is considered better than the reaction at 25 °C. Also, in order to choose the model reaction for the experiment, various solvents were tested (Table 5, entries 7–14). It is clear from entry 4 that the utilization of EtOH enhances the yield of the product (15 min, 93%). Finally, the best yield in a shorter time is found in the model reaction by applying just 0.015 g of SO₃H/NH₂NH₂/GPTMS/Fe₃O₄ in 2 mL of EtOH at 50 °C.

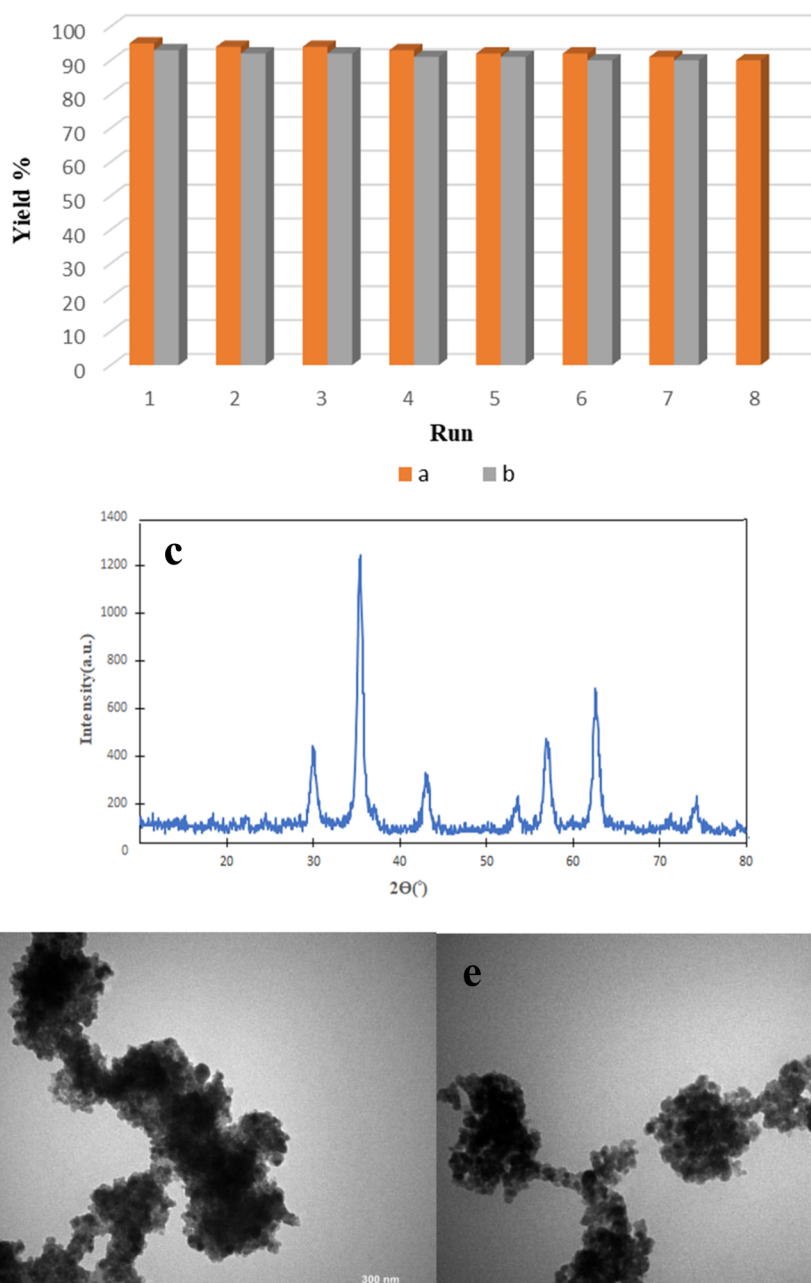


Figure 11. Reusability of the $\text{SO}_3\text{H}/\text{NH}_2\text{NH}_2/\text{GPTMS}/\text{Fe}_3\text{O}_4$ nanocatalyst in the preparation of (a) **4a** and (b) preparation of **7a**, (c) XRD, (d) TEM, and (e) TEM analyses of $\text{SO}_3\text{H}/\text{NH}_2\text{NH}_2/\text{GPTMS}/\text{Fe}_3\text{O}_4$ after 8 and 7 recycling experiments.

The higher activity of the $\text{SO}_3\text{H}/\text{NH}_2\text{NH}_2/\text{GPTMS}/\text{Fe}_3\text{O}_4$ catalyst compared with some other catalysts for the synthesis of product **7a** is indicated in Table 6. When H_2SO_4 (Table 6, entry 1), HSO_4Cl (Table 6, entry 2), Fe_3O_4 (Table 6, entry 4), FeCl_3 (Table 6, entry 5), $\text{FeSO}_4 \cdot 7\text{H}_2\text{O}$ (Table 6, entry 6), $\text{GPTMS}/\text{Fe}_3\text{O}_4$ (Table 6, entry 7), and $\text{NH}_2\text{NH}_2/\text{GPTMS}/\text{Fe}_3\text{O}_4$ (Table 6, entry 8) were employed as the catalyst, no yield was obtained for product **7a**, although the moderate yield (58%) was observed when $\text{SO}_3\text{H}/\text{NH}_2\text{NH}_2/\text{GPTMS}$ was used (Table 6, entry 3).

After optimization, a variety of electron-releasing and electron-withdrawing benzaldehydes were scrutinized for the preparation of derivatives of 3-pyrrolin-2-ones catalyzed by $\text{SO}_3\text{H}/\text{NH}_2\text{NH}_2/\text{GPTMS}/\text{Fe}_3\text{O}_4$ in order to identify the generality and the high proficiency of the catalytic system (Table 7).

Scheme 3 represents a logical mechanism to afford substituted 3-pyrrolin-2-ones in the presence of $\text{SO}_3\text{H}/\text{NH}_2\text{NH}_2/\text{GPTMS}/\text{Fe}_3\text{O}_4$ as an efficient, and reusable nanocatalyst. First, an imine is prepared during the reaction between aromatic aldehyde (**1**) and aniline (**5**). Next, diethyl acetylenedicarboxylate (**6**) during a nucleophilic addition with water forms a 1,3-dipolar intermediate and is added to the imine. Eventually, the desired product with nitrogen-containing five-membered ring (**7a–1**) is achieved through cyclization.

In the next stage, the reusability of the $\text{SO}_3\text{H}/\text{NH}_2\text{NH}_2/\text{GPTMS}/\text{Fe}_3\text{O}_4$ nanocatalyst was surveyed through the synthesis of substituted pyrans from dimedone, aldehydes derivatives, and malononitrile in the presence of 0.01 g of the catalyst under reflux conditions in a 1:1 mixture of $\text{H}_2\text{O}/\text{EtOH}$ and the preparation of substituted pyrrolidinone from aniline, aldehyde derivatives, and diethyl acetylenedicarboxylate in the

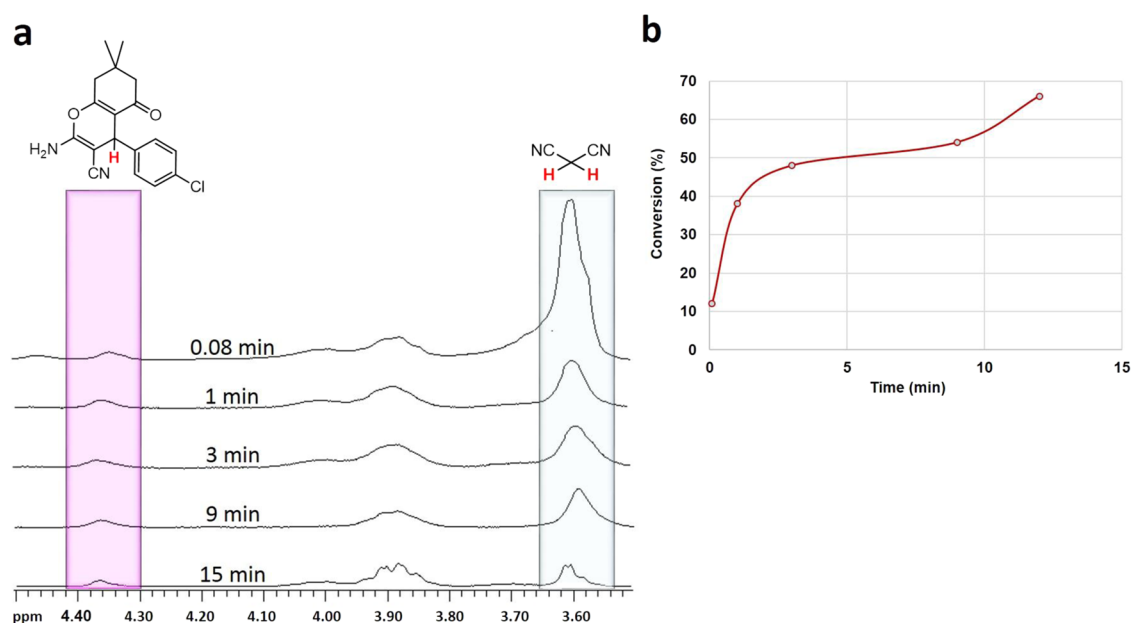


Figure 12. (a) Time-dependent ^1H NMR spectra recorded in CDCl_3 during the formation of 2-amino-4-(4-chlorophenyl)-7,7-dimethyl-5-oxo-5,6,7,8-tetrahydro-4H-chromene-3-carbonitrile from a reaction mixture of malononitrile (1.0 mmol), dimedone (1.0 mmol), and 4-chlorobenzaldehyde (1.0 mmol), using the $\text{SO}_3\text{H}/\text{NH}_2\text{NH}_2/\text{GPTMS}/\text{Fe}_3\text{O}_4$ nanocatalyst (0.01 g) in $\text{H}_2\text{O}/\text{EtOH}$ (1:1) (2 mL) under reflux. (b) Catalytic activity of $\text{SO}_3\text{H}/\text{NH}_2\text{NH}_2/\text{GPTMS}/\text{Fe}_3\text{O}_4$ according to the turnover frequency, employing a time below the 50% conversion level for a more accurate comparison (3 min). $\text{TOF} = (\text{mmol of 2-amino-4-(4-chlorophenyl)-7,7-dimethyl-5-oxo-5,6,7,8-tetrahydro-4H-chromene-3-carbonitrile})/(\text{mmol of sulfur in the catalyst} \times \text{time})$.

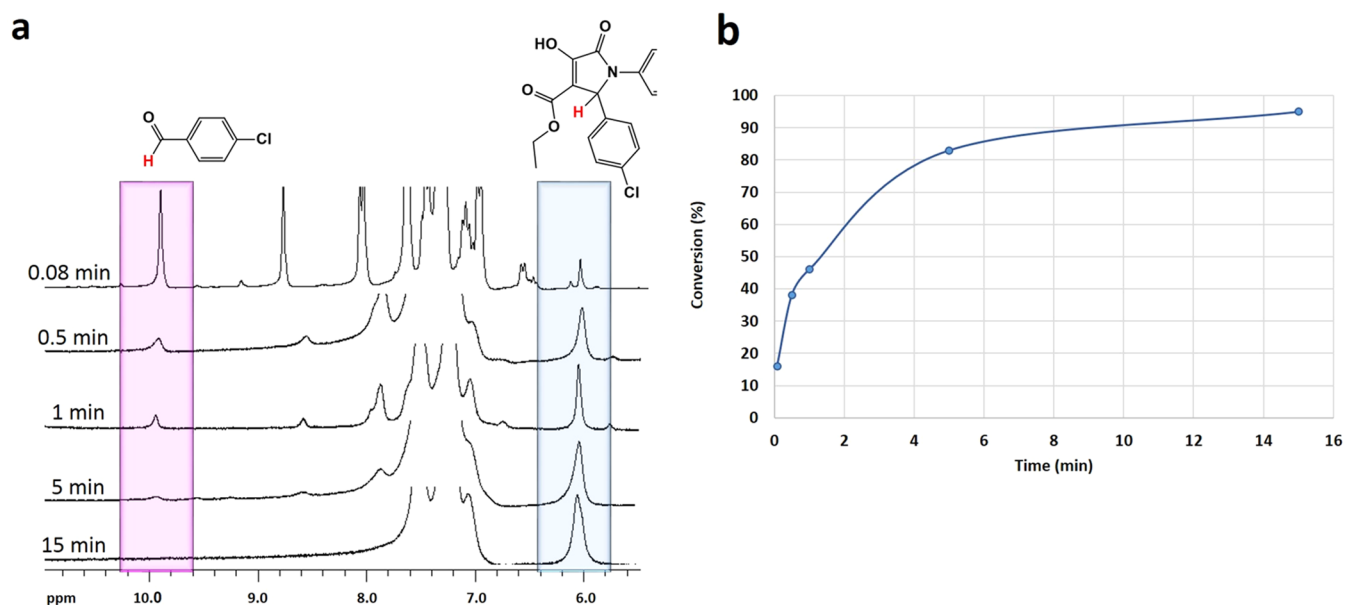


Figure 13. (a) Time-dependent ^1H NMR spectra recorded in DMSO during the formation of ethyl 2-(4-chlorophenyl)-4-hydroxy-5-oxo-1-phenyl-2,5-dihydro-1H-pyrrole-3-carboxylate from a reaction mixture of 4-chlorobenzaldehyde (1.0 mmol), aniline (1.0 mmol), and diethyl acetylenedicarboxylate (1.0 mmol) using a $\text{SO}_3\text{H}/\text{NH}_2\text{NH}_2/\text{GPTMS}/\text{Fe}_3\text{O}_4$ nanocatalyst (0.015 g) in EtOH (2 mL) at 50°C . (b) Catalytic activity of $\text{SO}_3\text{H}/\text{NH}_2\text{NH}_2/\text{GPTMS}/\text{Fe}_3\text{O}_4$ according to the turnover frequency, employing a time below the 50% conversion level for a more accurate comparison (1 min). $\text{TOF} = (\text{mmol of ethyl 2-(4-chlorophenyl)-4-hydroxy-5-oxo-1-phenyl-2,5-dihydro-1H-pyrrole-3-carboxylate})/(\text{mmol of sulfur in the catalyst} \times \text{time})$.

presence of 0.015 g of the catalyst in ethanol at 50°C . The nanocatalyst was reused for 8 cycles with the aim of preparing 4a and for 7 cycles aimed at preparing 7a according to the model reactions with an insignificant loss in its efficiency from 95 to 90% and from 93 to 90%, respectively (Figure 11). After recycling for 8 runs in the preparation of 4a and for 7 runs in the preparation of 7a, the XRD, TEM, and BET analyses for $\text{SO}_3\text{H}/$

$\text{NH}_2\text{NH}_2/\text{GPTMS}/\text{Fe}_3\text{O}_4$ were performed. The XRD analysis of $\text{SO}_3\text{H}/\text{NH}_2\text{NH}_2/\text{GPTMS}/\text{Fe}_3\text{O}_4$ after 8 runs is represented in Figure 11c. The average crystallite size of the reused catalyst is ~ 30.38 nm, obtained by the Debye–Scherrer equation. One can find TEM analyses of $\text{SO}_3\text{H}/\text{NH}_2\text{NH}_2/\text{GPTMS}/\text{Fe}_3\text{O}_4$ after 8 runs in the preparation of 4a and 7 runs of recycling in the preparation of 7a Figure 11d,e. The TEM image of the fresh

Table 8. Comparison of the Performance of SO₃H/NH₂NH₂/GPTMS/Fe₃O₄ with Those of Some Other Catalysts for the Formation of 4a^a

| entry | catalyst | condition | time (min) | yield (%) ^b | reference |
|-------|---|-------------------------------------|------------|------------------------|-----------|
| 1 | | H ₂ O/EtOH, reflux | 120 | 25 | |
| 2 | MNPs-PhSO ₃ H (0.01 g) | H ₂ O/EtOH (1:1), 100 °C | 15 | 90 | 62 |
| 3 | Fe ₃ O ₄ @SiO ₂ @5-SA (0.02 g) | H ₂ O, 60 °C | 100 | 92 | 63 |
| 4 | Fe ₃ O ₄ @g-C ₃ N ₄ (0.02 g) | EtOH, 60 °C | 60 | 95 | 64 |
| 5 | MNPs@Cu (10 mg) | solvent-free, 90 °C | 15 | 93 | 65 |
| 6 | DAHP (10 mol %) | H ₂ O/EtOH, 25 °C | 240 | 85 | 66 |
| 7 | Fe ₃ O ₄ /SiO ₂ -Met NPs (0.03 g) | H ₂ O/EtOH, reflux | 60 | 86 | 67 |
| 8 | t-ZrO ₂ NPs (10 mol %) | H ₂ O, 80 °C | 38 | 89 | 68 |
| 9 | urea (10 mol %) | H ₂ O/EtOH, 25 °C | 420 | 93 | 69 |
| 10 | Fe ₃ O ₄ @SiO ₂ @propyl-ANDSA | H ₂ O, reflux | 30 | 83 | 70 |
| 11 | KF/Al ₂ O ₃ (250 mg) | DMF, r.t. | 60–180 | 81 | 71 |
| 12 | Fe ₃ O ₄ @Ph-SO ₃ H (0.2 mol %) | H ₂ O, 50 °C | 25 | 88 | 72 |
| 13 | NiFe ₂ O ₄ @SiO ₂ @H ₁₄ [NaP ₃ W ₃₀ O ₁₁₀] (0.02 g) | EtOH, reflux | 20 | 67 | 73 |
| 14 | SO ₃ H/NH ₂ NH ₂ /GPTMS/Fe ₃ O ₄ | H ₂ O/EtOH, reflux | 15 | 95 | this work |

^aReaction conditions: 4-chlorobenzaldehyde (1 mmol), malononitrile (1 mmol) and dimedone (1 mmol), solvent (2 mL), and catalyst. ^bIsolated yield.

Table 9. Comparison of the Performance of SO₃H/NH₂NH₂/GPTMS/Fe₃O₄ with Those of Some Other Catalysts for the Preparation of 7a^a

| entry | catalyst | condition | time (min) | yield (%) ^b | reference |
|-------|---|-------------|------------|------------------------|-----------|
| 1 | | EtOH, 50 °C | 54 | | |
| 2 | CoFe ₂ O ₄ @silica-SO ₃ H (0.01 g) | EtOH, 60 °C | 720 | 90 | 61 |
| 3 | CoFe ₂ O ₄ @CA (75 mg) | EtOH, r.t. | 720 | 89 | 60 |
| 4 | citric acid monohydrate (2 mmol) | EtOH, r.t. | 600 | 86 | 27 |
| 5 | | lactic acid | 120 | 76 | 74 |
| 6 | | acetic acid | 120 | 33 | 74 |
| 7 | SO ₃ H/NH ₂ NH ₂ /GPTMS/Fe ₃ O ₄ | EtOH, 50 °C | 15 | 93 | this work |

^aReaction conditions: 4-chlorobenzaldehyde (1 mmol), aniline (1 mmol) and diethyl acetylenedicarboxylate (1 mmol), solvent (2 mL), catalyst. ^bIsolated yield.

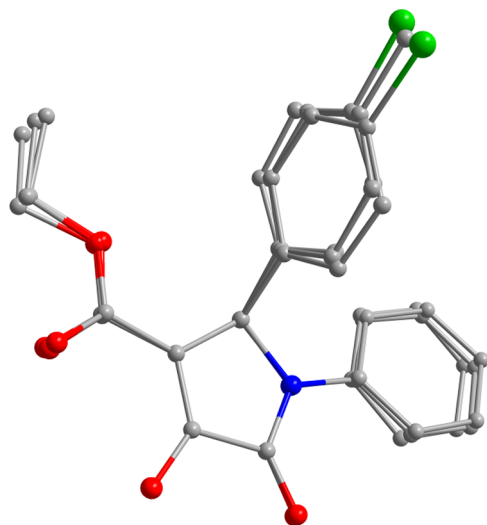


Figure 14. Comparison of the conformations of 7a (two different molecules) and 7d. The common reference points are pyrrole atoms. Hydrogen atoms are omitted for clarity. Color scheme: gray: C, blue: N, red: O, and green: Cl.

catalyst indicated the core–shell structure (Figure 6c) with a uniform size distribution diagram and an average size of 47–65 nm (Figure 6d). As can be seen, almost all SO₃H/NH₂NH₂/GPTMS/Fe₃O₄ particles with the same size and morphology as the fresh catalyst confirm the spherical shape and the size of

these particles is in the range of 50–69 nm. Furthermore, BET analyses for SO₃H/NH₂NH₂/GPTMS/Fe₃O₄ after 8 runs of recycling in the preparation of 4a and 7 runs of recycling in the preparation of 7a were performed. The total pore volume, surface area, and the mean pore diameter of SO₃H/NH₂NH₂/GPTMS/Fe₃O₄ after 8 runs of recycling in the preparation of 4a and 7 runs of recycling in the preparation of 7a were determined to be 0.1962 cm³ g⁻¹ and 33.031 m² g⁻¹, and 30.256 nm, and 0.2160 cm³ g⁻¹, 34.301 m² g⁻¹, and 32.500 nm, respectively.

As a case study, the ¹H NMR spectrum of the reaction mixture of malononitrile (1.0 mmol), dimedone (1.0 mmol), and 4-chlorobenzaldehyde (1.0 mmol) in H₂O/EtOH (1:1) (2 mL) under reflux was employed to investigate the catalytic activity of SO₃H/NH₂NH₂/GPTMS/Fe₃O₄, giving a turnover frequency of 504 h⁻¹ (Figure 12).

As a case study, the ¹H NMR spectrum of the reaction mixture of 4-chlorobenzaldehyde (1.0 mmol), aniline (1.0 mmol), and diethyl acetylenedicarboxylate (1.0 mmol) in EtOH (2 mL) at 50 °C was employed to investigate the catalytic activity of SO₃H/NH₂NH₂/GPTMS/Fe₃O₄, giving a turnover frequency of 1474 h⁻¹ (Figure 13).

As shown in Tables 8 and 9, the yields and reaction times were tabulated in order to compare the performance of SO₃H/NH₂NH₂/GPTMS/Fe₃O₄ with the results reported by some other catalysts for the formation of 4a and 7a. According to the results mentioned in Tables 8 and 9, it is clear that the short reaction time and high efficiency related to our method make this route useful as a protocol. Also, the new nanocatalyst has

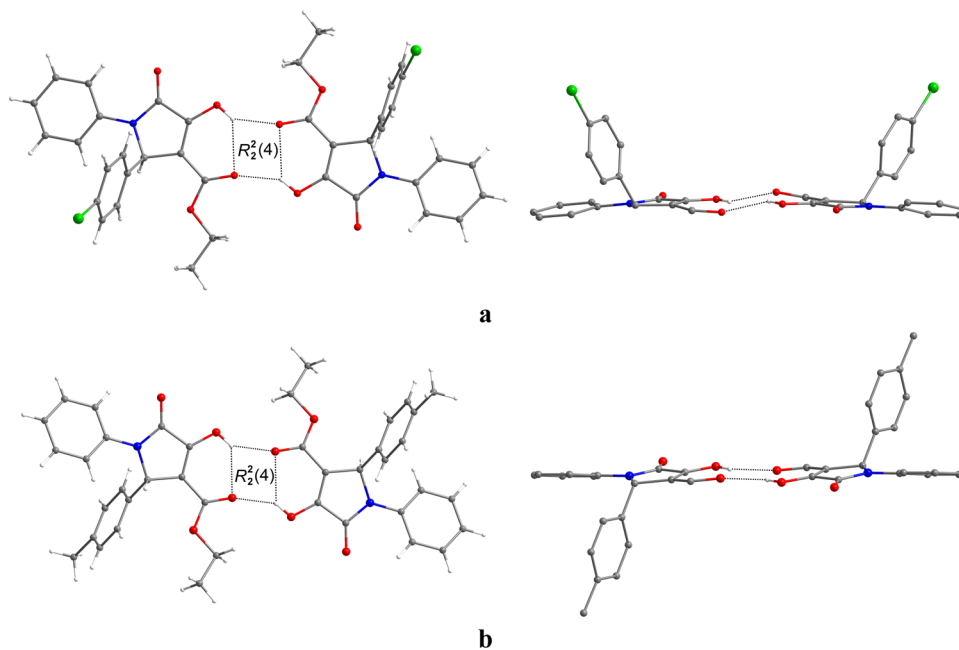


Figure 15. Non-centrosymmetric molecular dimer observed in 7a (a) compared with the centrosymmetric molecular dimer in 7d (b). Top (left panel) and side (right panel) views are shown. Hydrogen bonds are shown in black, dotted lines. Some of the atoms in the figures on the right panel are omitted for clarity. Color scheme: gray: C, white: H, blue: N, red: O, and green: Cl.

unique features such as easy separation, non-toxicity, and good stability.

The crystal structures of two compounds (7a and 7d) were confirmed by single-crystal X-ray analysis. Both crystals are centrosymmetric and contain racemic compounds. There is one molecule in the asymmetric unit of crystal 7d and two crystallographically different molecules in the crystal of 7a (asymmetric units with atom-numbering schemes of both structures are presented in Figure S1). Conformations of the three of them are almost the same (Figure 14). As previously observed in analogous compounds [66,106,118,120,121,135,136], in the case of both crystals presented here, molecules form dimers via O–H...O hydrogen bonds giving intradimeric $R_2^2(4)$ ring motifs (centrosymmetric in 7d and non-centrosymmetric in 7a) (Figure 15). Chlorine atom in 7a is involved in the formation of hydrogen bonds with the CH group of the phenyl ring (Figure S2). Also, some details of the geometry of selected hydrogen bonds and selected geometric parameters are given in Tables S2 and S3.

4. CONCLUSIONS

SO₃H-functionalized epoxy-immobilized Fe₃O₄ core-shell MNPs as an effectual, reusable, and eco-friendly nanocatalyst was applied for the sustainable and green synthesis of pyran and pyrrolidinone derivatives. This synthesized nanocatalyst was prepared by employing a three-step procedure and investigated by utilizing FT-IR, BET, EDX, PXRD, SEM, VSM, TGA, TEM, and DTG. The isolation of the nanocatalyst from the reaction mixtures was carried out simply by applying a simple external magnetic field and reused for 8 cycles in the preparation of tetrahydrobenzo[*b*]pyran and 7 runs in the preparation of 3-pyrrolin-2-ones according to the model reactions with an insignificant loss in its efficiency. Some amazing advantages of the present methodology are the use of a recyclable and easily reusable catalyst, mild reaction conditions, use of a green solvent, eco-friendliness, low catalyst loading, and separation of

products from the reaction mixtures without the requirement of a chromatographic column in high to excellent yields.

■ ASSOCIATED CONTENT

Supporting Information

The Supporting Information is available free of charge at <https://pubs.acs.org/doi/10.1021/acsomega.3c01068>.

Copies of FT-IR, ¹H NMR, and ¹³C NMR spectra, and crystallographic data for some synthesized products (PDF)

■ AUTHOR INFORMATION

Corresponding Author

Ali Ramazani – Department of Chemistry, University of Zanjan, Zanjan 45371-38791, Iran; Department of Biotechnology, Research Institute of Modern Biological Techniques (RIMBT), University of Zanjan, Zanjan 45371-38791, Iran; orcid.org/0000-0003-3072-7924; Email: aliramazani@gmail.com, aliramazani@znu.ac.ir

Authors

Fatemeh Kalantari – Department of Chemistry, University of Zanjan, Zanjan 45371-38791, Iran
 Hussein Esmailipour – Department of Chemistry, University of Zanjan, Zanjan 45371-38791, Iran
 Hamideh Ahankar – Department of Chemistry, Abhar Branch, Islamic Azad University, Abhar 45619-33367, Iran
 Hamideh Aghahosseini – Department of Chemistry, University of Zanjan, Zanjan 45371-38791, Iran
 Oskar Kaszubowski – Faculty of Chemistry, University of Wrocław, 50-383 Wrocław, Poland; orcid.org/0000-0002-1650-2975
 Katarzyna Ślepokura – Faculty of Chemistry, University of Wrocław, 50-383 Wrocław, Poland; orcid.org/0000-0001-8330-4218

Complete contact information is available at:

https://pubs.acs.org/10.1021/acsomega.3c01068

Notes

The authors declare no competing financial interest.

ACKNOWLEDGMENTS

This work was supported by the Iran National Science Foundation.

REFERENCES

- (1) Hoener, C. F.; Allan, K. A.; Bard, A. J.; Campion, A.; Fox, M. A.; Mallouk, T. E.; Webber, S. E.; White, J. M. Demonstration of a shell-core structure in layered cadmium selenide-zinc selenide small particles by x-ray photoelectron and Auger spectroscopies. *J. Phys. Chem. A* **1992**, *96*, 3812–3817.
- (2) Tartaj, P.; Morales, M. P.; Gonzalez-Carreño, T.; Veintemillas-Verdaguer, S.; Serna, C. J. The iron oxides strike back: from biomedical applications to energy storage devices and photoelectrochemical water splitting. *Adv. Mater.* **2011**, *23*, 5243–5249.
- (3) Shiri, L.; Ghorbani-Choghamarani, A.; Kazemi, M. Sulfides synthesis: nanocatalysts in C–S cross-coupling reactions. *Aust. J. Chem.* **2016**, *69*, 585–600.
- (4) Ghorbani-Choghamarani, A.; Norouzi, M. Synthesis of copper (II)-supported magnetic nanoparticle and study of its catalytic activity for the synthesis of 2, 3-dihydroquinazolin-4 (1H)-ones. *J. Mol. Catal. A* **2014**, *395*, 172–179.
- (5) Vayssières, L.; Chanéac, C.; Tronc, E.; Jolivet, J. P. Size tailoring of magnetite particles formed by aqueous precipitation: an example of thermodynamic stability of nanometric oxide particles. *J. Colloid Interface Sci.* **1998**, *205*, 205–212.
- (6) Chen, M.-N.; Mo, L.-P.; Cui, Z.-S.; Zhang, Z.-H. Magnetic nanocatalysts: synthesis and application in multicomponent reactions. *Curr. Opin. Green Sustainable Chem.* **2019**, *15*, 27–37.
- (7) Gao, G.; Di, J.-Q.; Zhang, H.-Y.; Mo, L.-P.; Zhang, Z.-H. A magnetic metal organic framework material as a highly efficient and recyclable catalyst for synthesis of cyclohexenone derivatives. *J. Catal.* **2020**, *387*, 39–46.
- (8) Kazemi, M.; Shiri, L.; Kohzadi, H. Recent advances in aryl alkyl and dialkyl sulfide synthesis. *Phosphorus, Sulfur Silicon Relat. Elem.* **2015**, *190*, 978–1003.
- (9) Sheykhan, M.; Ma'mani, L.; Ebrahimi, A.; Heydari, A. Sulfamic acid heterogenized on hydroxyapatite-encapsulated γ -Fe₂O₃ nanoparticles as a magnetic green interphase catalyst. *J. Mol. Catal. A* **2011**, *335*, 253–261.
- (10) Terada, M.; Sorimachi, K. Enantioselective Friedel–Crafts reaction of electron-rich alkenes catalyzed by chiral Brønsted acid. *J. Am. Chem. Soc.* **2007**, *129*, 292–293.
- (11) Ogoshi, T.; Kanai, S.; Fujinami, S.; Yamagishi, T.-a.; Nakamoto, Y. para-Bridged symmetrical pillar [5] arenes: their Lewis acid catalyzed synthesis and host–guest property. *J. Am. Chem. Soc.* **2008**, *130*, 5022–5023.
- (12) Muratore, M. E.; Holloway, C. A.; Pilling, A. W.; Storer, R. I.; Trevitt, G.; Dixon, D. J. Enantioselective Brønsted acid-catalyzed N-acyliminium cyclization cascades. *J. Am. Chem. Soc.* **2009**, *131*, 10796–10797.
- (13) Shubayev, V. I.; Pisanic, T. R., II; Jin, S. Magnetic nanoparticles for theragnostics. *Adv. Drug Delivery Rev.* **2009**, *61*, 467–477.
- (14) Liu, J.; Qiao, S. Z.; Hu, Q. H.; Lu, G. Q. Magnetic nanocomposites with mesoporous structures: synthesis and applications. *Small* **2011**, *7*, 425–443.
- (15) Mahmoudi, H.; Jafari, A. A.; Saeedi, S.; Firouzabadi, H. Sulfonic acid-functionalized magnetic nanoparticles as a recyclable and eco-friendly catalyst for atom economical Michael addition reactions and bis indolyl methane synthesis. *RSC Adv.* **2015**, *5*, 3023–3030.
- (16) Zhang, X.; Zhang, L.; Yang, Q. Designed synthesis of sulfonated polystyrene/mesoporous silica hollow nanospheres as efficient solid acid catalysts. *J. Mater. Chem. A* **2014**, *2*, 7546–7554.
- (17) Esquivel, D.; Jiménez-Sanchidrián, C.; Romero-Salguero, F. J. Thermal behaviour, sulfonation and catalytic activity of phenylene-bridged periodic mesoporous organosilicas. *J. Mater. Chem.* **2011**, *21*, 724–733.
- (18) Melero, J. A.; Stucky, G. D.; van Grieken, R.; Morales, G. Direct syntheses of ordered SBA-15 mesoporous materials containing arenesulfonic acid groups. *J. Mater. Chem.* **2002**, *12*, 1664–1670.
- (19) Khorshidi, A.; Shariati, S. Efficient synthesis of 3, 3'-bisindoles catalyzed by Fe₃O₄@ MCM-48-OSO₃H magnetic core-shell nanoparticles. *Chin. J. Catal.* **2015**, *36*, 778–784.
- (20) Esfahani, F. K.; Zareyee, D.; Yousefi, R. Sulfonated core-shell magnetic nanoparticle (Fe₃O₄@SiO₂@ PrSO₃H) as a highly active and durable protonic acid catalyst; synthesis of coumarin derivatives through Pechmann reaction. *ChemCatChem* **2014**, *6*, 3333–3337.
- (21) Van Rhijn, W. M.; De Vos, D.; Sels, B.; Bossaert, W. Sulfonic acid functionalised ordered mesoporous materials as catalysts for condensation and esterification reactions. *Chem. Commun.* **1998**, *3*, 317–318.
- (22) Modarresi-Alam, A. R.; Inaloo, I. D.; Kleinpeter, E. Synthesis of primary thiocarbamates by silica sulfuric acid as effective reagent under solid-state and solution conditions. *J. Mol. Struct.* **2012**, *1024*, 156–162.
- (23) Sardarian, A. R.; Inaloo, I. D. 4-Dodecylbenzenesulfonic acid (DBSA) promoted solvent-free diversity-oriented synthesis of primary carbamates, S-thiocarbamates and ureas. *RSC Adv.* **2015**, *5*, 76626–76641.
- (24) Sardarian, A. R.; Inaloo, I. D.; Modarresi-Alam, A. R.; Kleinpeter, E.; Schilde, U. Metal-free regioselective monocyanoation of hydroxy-, alkoxy-, and benzyloxyarenes by potassium thiocyanate and silica sulfuric acid as a cyanating agent. *J. Org. Chem.* **2019**, *84*, 1748–1756.
- (25) Inaloo, I. D.; Majnooni, S. Eco-Efficient Ultrasonic-Responsive Synthesis of Primary O-Alkyl and O-Aryl Thiocarbamates Using Brønsted Acid Ionic Liquid [H-NMP][HSO₄] in Aqueous Media at Room Temperature. *ChemistrySelect* **2018**, *3*, 4095–4100.
- (26) Fardood, S. T.; Ramazani, A. Green synthesis and characterization of copper oxide nanoparticles using coffee powder extract. *J. Nanostruct.* **2016**, *6*, 167–171.
- (27) Ahankar, H.; Ramazani, A.; Ślepokura, K.; Lis, T.; Joo, S. W. Synthesis of pyrrolidinone derivatives from aniline, an aldehyde and diethyl acetylenedicarboxylate in an ethanolic citric acid solution under ultrasound irradiation. *Green Chem.* **2016**, *18*, 3582–3593.
- (28) Kalantari, F.; Rezayati, S.; Ramazani, A.; Aghahosseini, H.; Ślepokura, K.; Lis, T. Proline-cu complex based 1,3,5-triazine coated on Fe₃O₄ magnetic nanoparticles: a nanocatalyst for the Knoevenagel condensation of aldehyde with malononitrile. *ACS Appl. Nano Mater.* **2022**, *5*, 1783–1797.
- (29) Nasseri, M. A.; Sadeghzadeh, S. M. Magnetic nanoparticle supported hyperbranched polyglycerol catalysts for synthesis of 4 H-benzo [b] pyran. *Monatsh. Chem.* **2013**, *144*, 1551–1558.
- (30) Khare, S. P.; Deshmukh, T. R.; Akolkar, S. V.; Sangshetti, J. N.; Khedkar, V. M.; Shingate, B. B. New 1, 2, 3-triazole-linked tetrahydrobenzo [b] pyran derivatives: Facile synthesis, biological evaluation and molecular docking study. *Res. Chem. Intermed.* **2019**, *45*, 5159–5182.
- (31) Zolfigol, M. A.; Khazaei, A.; Moosavi-Zare, A. R.; Afsar, J.; Khakyzadeh, V.; Khaledian, O. Knoevenagel-Michael-cyclocondensation Tandem Reaction of Malononitrile, Various Aldehydes and Dimedone Catalyzed by Sulfonic Acid Functionalized Pyridinium Chloride as a New Ionic Liquid and Catalyst. *J. Chin. Chem. Soc.* **2015**, *62*, 398–403.
- (32) Moosavi-Zare, A. R.; Zolfigol, M. A.; Khaledian, O.; Khakyzadeh, V.; Farahani, M. D.; Kruger, H. G. Tandem Knoevenagel–Michael-cyclocondensation reactions of malononitrile, various aldehydes and dimedone using acetic acid functionalized ionic liquid. *New J. Chem.* **2014**, *38*, 2342–2347.
- (33) Kangani, M.; Maghsoodlou, M.-T.; Hazeri, N. Vitamin B12: An efficient type catalyst for the one-pot synthesis of 3, 4, 5-trisubstituted furan-2 (5H)-ones and N-aryl-3-aminodihydropyrrrol-2-one-4-carboxylates. *Chin. Chem. Lett.* **2016**, *27*, 66–70.

- (34) Shiozawa, H.; Takahashi, S. Configurational studies on thiomarinol. *J. Antibiot.* **1994**, *47*, 851–853.
- (35) Ettlinger, L.; Gäumann, E.; Hütter, R.; Keller-Schierlein, W.; Kradolfer, F.; Neipp, L.; Prelog, V.; Zähler, H. Stoffwechselprodukte von Actinomyceten 17. Mitteilung Holomycin. *Helv. Chim. Acta* **1959**, *42*, 563–569.
- (36) Omura, S.; Fujimoto, T.; Otoguro, K.; Matsuzaki, K.; Moriguchi, R.; Tanaka, H.; Sasaki, Y. Lactacystin, a novel microbial metabolite, induces neuritogenesis of neuroblastoma cells. *J. Antibiot.* **1991**, *44*, 113–116.
- (37) Zhu, Q.; Gao, L.; Chen, Z.; Zheng, S.; Shu, H.; Li, J.; Jiang, H.; Liu, S. A novel class of small-molecule caspase-3 inhibitors prepared by multicomponent reactions. *Eur. J. Med. Chem.* **2012**, *54*, 232–238.
- (38) Brine, G. A.; Boldt, K. G. Synthesis and anticonvulsant screening of 3, 3-diphenyl-2-pyrrolidone derivatives. *J. Pharm. Sci.* **1983**, *72*, 700–702.
- (39) Yuan, D.; Zhang, Q.; Dou, J. Supported nanosized palladium on superparamagnetic composite microspheres as an efficient catalyst for Heck reaction. *Catal. Commun.* **2010**, *11*, 606–610.
- (40) Tural, B.; Tural, S.; Ertaş, E.; Yalınkılıç, İ.; Demir, A. S. Purification and covalent immobilization of benzaldehyde lyase with heterofunctional chelate-epoxy modified magnetic nanoparticles and its carboligation reactivity. *J. Mol. Catal. B* **2013**, *95*, 41–47.
- (41) Naeimi, H.; Nazifi, Z. S. A highly efficient nano-Fe₃O₄ encapsulated-silica particles bearing sulfonic acid groups as a solid acid catalyst for synthesis of 1, 8-dioxo-octahydroxanthene derivatives. *J. Nanopart. Res.* **2013**, *15*, 2026.
- (42) *CrysAlisPRO in Xcalibur R Software*; Agilent Technologies: Yarnton, U.K., 2012.
- (43) Sheldrick, G. M. SHELXT—Integrated space-group and crystal-structure determination. *Acta Crystallogr., Sect. A* **2015**, *71*, 3–8.
- (44) Sheldrick, G. M. Crystal structure refinement with SHELXL. *Acta Crystallogr., Sect. C* **2015**, *71*, 3–8.
- (45) Groom, C. R.; Allen, F. H. The Cambridge Structural Database in retrospect and prospect. *Angew. Chem., Int. Ed.* **2014**, *53*, 662–671.
- (46) Sun, J.; W, Q.; Xia, E.-Y.; Yan, C.-G. Molecular Diversity of Three-Component Reactions of Aromatic Aldehydes, Arylamines, and Acetylenedicarboxylates. *Eur. J. Org. Chem.* **2011**, *2011*, 2981–2986.
- (47) *XP-Interactive Molecular Graphics*; Bruker Analytical X-ray Systems: Madison, 1998.
- (48) Brandenburg, K. *DIAMOND, version 3.0*; Crystal Impact GbR: Bonn, Germany, 2005.
- (49) Chen, H.; Huang, Z.; Hu, X.; Tang, G.; Xu, P.; Zhao, Y.; Cheng, C.-H. Nickel-catalyzed cross-coupling of aryl phosphates with arylboronic acids. *J. Org. Chem.* **2011**, *76*, 2338–2344.
- (50) Chary, K. V. R.; Srikanth, C. S. Selective hydrogenation of nitrobenzene to aniline over Ru/SBA-15 catalysts. *Catal. Lett.* **2009**, *128*, 164–170.
- (51) Kazemzad, M.; Yuzbashi, A. A.; Balalaie, S.; Bararjanian, M. Modified SBA-15 as an efficient environmentally friendly nanocatalyst for one-pot synthesis of tetrahydrobenzo [b] pyrane derivatives. *Synth. React. Inorg., Met.-Org., and Nano-Met. Chem.* **2011**, *41*, 1182–1187.
- (52) Kalantari, F.; Ramazani, A.; Poor Heravi, M. R.; Aghahosseini, H.; Slepokura, K. Magnetic Nanoparticles Functionalized with Copper Hydroxyproline Complexes as an Efficient, Recoverable, and Recyclable Nanocatalyst: Synthesis and Its Catalytic Application in a Tandem Knoevenagel–Michael Cyclocondensation Reaction. *Inorg. Chem.* **2021**, *60*, 15010–15023.
- (53) Maleki, B.; Ashrafi, S. S. Nano α -Al₂O₃ supported ammonium dihydrogen phosphate (NH₄H₂PO₄/Al₂O₃): preparation, characterization and its application as a novel and heterogeneous catalyst for the one-pot synthesis of tetrahydrobenzo [b] pyran and pyrano [2, 3-c] pyrazole derivatives. *RSC Adv.* **2014**, *4*, 42873–42891.
- (54) Baghbanian, S. M.; Rezaei, N.; Tashakkorian, H. Nanozeolite clinoptilolite as a highly efficient heterogeneous catalyst for the synthesis of various 2-amino-4 H-chromene derivatives in aqueous media. *Green Chem.* **2013**, *15*, 3446–3458.
- (55) Shamsi, T.; Amoozadeh, A.; Sajjadi, S. M.; Tabrizian, E. Novel type of SO₃H–functionalized nano-titanium dioxide as a highly efficient and recyclable heterogeneous nanocatalyst for the synthesis of tetrahydrobenzo [b] pyrans. *Appl. Organomet. Chem.* **2017**, *31*, No. e3636.
- (56) Balalaie, S.; Bararjanian, M.; Amani, A. M.; Movassagh, B. (S)-Proline as a neutral and efficient catalyst for the one-pot synthesis of tetrahydrobenzo [b] pyran derivatives in aqueous media. *Synlett* **2006**, *2006*, 263–266.
- (57) Gao, S.; Tsai, C. H.; Tseng, C.; Yao, C.-F. Fluoride ion catalyzed multicomponent reactions for efficient synthesis of 4H-chromene and N-arylquinoline derivatives in aqueous media. *Tetrahedron* **2008**, *64*, 9143–9149.
- (58) Ahankar, H.; Ramazani, A.; Ślepokura, K.; Kinzhybaloe, V. Malic acid as an effective and valuable bioorganocatalyst for one-pot, three-component synthesis of pyrrolidinone derivatives. *Arxiv* **2022**, 27–40.
- (59) Dutta, A.; Rohman, M. A.; Nongrum, R.; Thongni, A.; Mitra, S.; Nongkhaw, R. Visible light-promoted synthesis of pyrrolidinone derivatives via Rose Bengal as a photoredox catalyst and their photophysical studies. *New J. Chem.* **2021**, *45*, 8136–8148.
- (60) Ahankar, H.; Ramazani, A.; Ślepokura, K.; Lis, T.; Kinzhybaloe, V. Magnetic cobalt ferrite nanoparticles functionalized with citric acid as a green nanocatalyst for one-pot three-component sonochemical synthesis of substituted 3-pyrrolin-2-ones. *Res. Chem. Intermed.* **2019**, *45*, 5007–5025.
- (61) Hosseinzadeh, Z.; Ramazani, A.; Ahankar, H.; Ślepokura, K.; Lis, T. Sulfonic acid-functionalized silica-coated magnetic nanoparticles as a reusable catalyst for the preparation of pyrrolidinone derivatives under eco-friendly conditions. *Silicon* **2019**, *11*, 2933–2943.
- (62) Faroughi Niya, H.; Hazeri, N.; Rezaie Kahkhaie, M.; Maghsoodlou, M. T. Preparation and characterization of MNPs–PhSO₃H as a heterogeneous catalyst for the synthesis of benzo [b] pyran and pyrano [3, 2-c] chromenes. *Res. Chem. Intermed.* **2020**, *46*, 1685–1704.
- (63) Saboury, F.; Azizi, N.; Mirjafari, Z.; Mahmoudi Hashemi, M. A general and inexpensive protocol for the nanomagnetic 5-sulfosalicylic acid catalyzed the synthesis of tetrahydrobenzo [b] pyrans and quinoxaline derivatives. *J. Iran. Chem. Soc.* **2020**, *17*, 2533–2543.
- (64) Azizi, N.; Ahoie, T. S.; Hashemi, M. M.; Yavari, I. Magnetic graphitic carbon nitride-catalyzed highly efficient construction of functionalized 4H-pyrans. *Synlett* **2018**, *29*, 645–649.
- (65) Ma, W.; Ebadi, A. G.; Javahershenas, R.; Javahershenas, R.; Jimenez, G. One-pot synthesis of 2-amino-4 H-chromene derivatives by MNPs@Cu as an effective and reusable magnetic nanocatalyst. *RSC Adv.* **2019**, *9*, 12801–12812.
- (66) Sabitha, G.; Arundhathi, K.; Sudhakar, K.; Sastry, B.; Yadav, J. Cerium (III) chloride–catalyzed one-pot synthesis of tetrahydrobenzo [b] pyrans. *Synth. Commun.* **2009**, *39*, 433–442.
- (67) Alizadeh, A.; Khodaei, M. M.; Beygzadeh, M.; Kordestani, D.; Feyzi, M. Biguanide-functionalized Fe₃O₄/SiO₂ magnetic nanoparticles: an efficient heterogeneous organosuperbase catalyst for various organic transformations in aqueous media. *Bull. Korean Chem. Soc.* **2012**, *33*, 2546–2552.
- (68) Saha, A.; Payra, S.; Banerjee, S. On water synthesis of pyran–chromenes via a multicomponent reactions catalyzed by fluorescent t-ZrO₂ nanoparticles. *RSC Adv.* **2015**, *5*, 101664–101671.
- (69) Brahmachari, G.; Banerjee, B. Facile and one-pot access to diverse and densely functionalized 2-amino-3-cyano-4 H-pyrans and pyran-annulated heterocyclic scaffolds via an eco-friendly multi-component reaction at room temperature using urea as a novel organo-catalyst. *ACS Sustainable Chem. Eng.* **2014**, *2*, 411–422.
- (70) Sanati, H.; Karamshahi, Z.; Ghorbani-Vaghei, R. Fe₃O₄@SiO₂@Propyl–ANDSA: as a new catalyst for one-pot synthesis of 4H-chromene. *Res. Chem. Intermed.* **2019**, *45*, 709–726.
- (71) Wang, X.-S.; Shi, D.-Q.; Tu, S.-J.; Yao, C.-S. A convenient synthesis of 5-Oxo-5, 6, 7, 8-tetrahydro-4 H-benzo-[b]-pyran derivatives catalyzed by KF-Alumina. *Synth. Commun.* **2003**, *33*, 119–126.
- (72) Elhamifar, D.; Ramazani, Z.; Norouzi, M.; Mirbagheri, R. Magnetic iron oxide/phenylsulfonic acid: a novel, efficient and

recoverable nanocatalyst for green synthesis of tetrahydrobenzo [b] pyrans under ultrasonic conditions. *J. Colloid Interface Sci.* **2018**, *511*, 392–401.

(73) Maleki, B.; Baghayeri, M.; Abadi, S. A. J.; Tayebee, R.; Khojastehnezhad, A. Ultrasound promoted facile one pot synthesis of highly substituted pyran derivatives catalyzed by silica-coated magnetic NiFe₂O₄ nanoparticle-supported H₁₄ [NaP₅W₃₀O₁₁₀] under mild conditions. *RSC Adv.* **2016**, *6*, 96644–96661.

(74) Yang, J.; Tan, J.-N.; Gu, Y. Lactic acid as an invaluable bio-based solvent for organic reactions. *Green Chem.* **2012**, *14*, 3304–3317.

■ NOTE ADDED AFTER ASAP PUBLICATION

Table 7 title was corrected July 10, 2023.